NASA TN D-1622



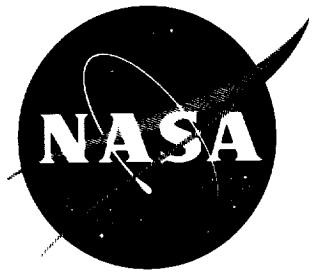


# TECHNICAL NOTE

D-1622

## REAL-GAS EFFECTS ON HYPERSONIC NOZZLE CONTOURS WITH A METHOD OF CALCULATION

By Charles B. Johnson, Lillian R. Boney,
James C. Ellison, and Wayne D. Erickson

Langley Research Center
Langley Station, Hampton, Va.

NATIONAL AERONAUTICS AND SPACE ADMINISTRATION

WASHINGTON April 1963

Code - 1

NATIONAL AERONAUTICS AND SPACE ADMINISTRATION

TECHNICAL NOTE D-1622

# REAL-GAS EFFECTS ON HYPERSONIC NOZZLE CONTOURS WITH A METHOD OF CALCULATION

By Charles B. Johnson, Lillian R. Boney,
James C. Ellison, and Wayne D. Erickson



## SUMMARY

A method is presented for computing the wall coordinates of a hypersonic nozzle with real-gas[1] effects. Results of calculations at a Mach number of 17 for stagnation temperatures and pressures up to 5,000° R and 1,000 atmospheres are presented. A procedure for calculating both the inviscid contour and boundary-layer displacement thickness is presented along with a complete computer program written in FORTRAN (FORmula TRANslation) language. Calculations are presented for a Mach number 17 nozzle for nitrogen at various stagnation conditions to indicate the difference between the use of real-gas properties and the ideal gas with constant heat-capacity ratio. The effect of stagnation conditions on both the inviscid flow field and the growth of the displacement thickness has been investigated. Whereas the present results were obtained for nitrogen, the method of calculation presented herein could be applied to other gases with only slight modification.

## INTRODUCTION

The calculation of the inviscid contour of a hypersonic nozzle for a real gas involves an application of the method of characteristics in which the real-gas variation of the thermodynamic properties of the gas are considered. The physical-wall contour of the nozzle is then determined by adding the calculated displacement thickness to the inviscid contour.

In reference 1 a procedure is presented for calculating only the inviscid contour of axisymmetric nozzles with reacting gases by application of the method of characteristics incorporating a variable isentropic exponent, whereas, in the present work the available thermodynamic data for an isentropic expansion are used directly in the computation scheme. The method for calculating the contour of axisymmetric nozzles for high-temperature air presented in reference 2 is similar to that presented herein but was developed independently. The differences between the present work and that of reference 2 include the manner in which the

[1]The term "real gas" as used herein relates to the effects associated with high densities and also the variation of heat capacity with temperature.

real-gas thermodynamic properties are employed and the detailed calculation procedures for the boundary-layer determination.

A comparison between the calculated inviscid coordinates of a hypersonic nozzle based on the real-gas thermodynamic properties of air at moderately high stagnation temperature and pressure and the coordinates based on ideal-gas relations with constant heat capacity indicates that real-gas effects strongly affect the calculated nozzle contour. (See ref. 3.)

The procedure for calculating the wall contour of a hypersonic nozzle presented in this report was used to design the nozzle of a Mach number 17 hypersonic facility which is presently being constructed for the Langley Research Center. This facility is to operate with nitrogen at stagnation temperatures up to 4,000° F and stagnation pressures up to 1,000 atmospheres for running times on the order of minutes and has a test-section diameter of approximately 17 inches.

It is the main objective of this report to present a method for calculating the physical-wall coordinates of a hypersonic nozzle which operates under conditions where real-gas effects are significant. In addition to the method of calculation, a comparison is given between the contours determined by inclusion of real-gas effects and of ideal-gas considerations with constant heat capacities for various stagnation conditions. The effect of wall temperature, size of integration step, and other calculational restraints are also discussed.

The method of calculation will be presented in enough detail to permit the direct use of this approach for determining the physical-wall contour of a hypersonic nozzle for a wide range of conditions. The modifications to this method which would be required for dealing with gases other than nitrogen and for considerably different conditions are also listed.

## SYMBOLS

| | |
|---|---|
| $a$ | velocity of sound |
| $B,C,D$ | points in axisymmetric flow field as indicated in sketch (a); used as subscripts to indicate conditions at these points |
| $C_f$ | skin-friction coefficient |
| $d^*$ | throat diameter |
| $H$ | total enthalpy |
| $h$ | static enthalpy |
| $M$ | Mach number |
| $N$ | exponent in velocity-profile relation |

| | |
|---|---|
| $N_{Re}$ | local Reynolds number based on momentum thickness $\theta$ |
| $p$ | pressure |
| $Q$ | enthalpy correction term |
| $R$ | gas constant for nitrogen |
| $r$ | distance from source point in radial flow field |
| $r_{cr}$ | distance from source point to sonic sphere in radial flow |
| $r'$ | radial distance from nozzle axis |
| $s$ | distance along Mach line measured in meridian plane from nozzle axis |
| $T$ | temperature |
| $T_b$ | base temperature, $491.688^\circ$ R |
| $T_r$ | gas temperature at nozzle throat (see eq. (B16)) |
| $u$ | velocity |
| $u_l$ | limiting velocity |
| $u'$ | velocity in $\tilde{x}$ direction |
| $W$ | limiting velicity ratio, $W = \frac{u}{u_l}$ |
| $x$ | distance along nozzle axis with $x = 0$ at nozzle throat |
| $\bar{x}$ | distance from source point of radial flow parallel to nozzle axis |
| $\tilde{x}$ | distance measured parallel to nozzle wall with $\tilde{x} = 0$ at nozzle throat |
| $y$ | distance perpendicular to nozzle axis |
| $\tilde{y}$ | distance measured perpendicular to nozzle wall with $\tilde{y} = 0$ at nozzle wall |
| $y^*$ | nozzle throat height, $\frac{d^*}{2}$ |
| $\gamma$ | ratio of specific heats |
| $\delta$ | boundary-layer thickness |

$\delta^*$ boundary-layer displacement thickness, defined by equation (B2)

$\Theta$ characteristic temperature of molecular vibration for nitrogen, $6{,}005.9^\circ$ R

$\theta$ momentum thickness

$\theta_f$ flow angle

$\theta_I$ integrated values of flow angle, $\theta_I = \int_0^{\theta_{f,I}} d\theta_f$, as given in equation (A6)

$\theta^*$ initial value of $\theta$ at nozzle throat

$\mu$ Mach angle

$\rho$ density

$\psi$ stream function

$\bar{\psi}$ nondimensional stream function, see equation (A9)

$\omega$ viscosity-temperature exponent

Subscripts:

aw adiabatic-wall condition

L edge of laminar sublayer

t stagnation conditions

w wall condition

1 inviscid free-stream conditions

Superscript:

o condition of low pressure

## METHOD OF CALCULATION

The calculation of a real-gas nozzle contour is based on a characteristic solution for determining the inviscid flow field and then adding a correction of boundary-layer displacement thickness to the inviscid nozzle contour. In the method presented herein, the actual thermodynamic properties of the expanding gas

are used to determine the inviscid flow-field boundary. A detailed procedure for calculating the inviscid portion of a hypersonic nozzle is presented in appendix A.

After the inviscid contour has been determined by the procedure of appendix A, a displacement thickness based on real-gas properties is calculated from the edge of the inviscid contour to a physical wall. This calculation is based on a turbulent boundary-layer analysis in which the real-gas flow properties are used in a stepwise integration of the axisymmetric form of the momentum equation. (See pp. 393 to 395 of ref. 4.) The heat transfer to the nozzle wall is accounted for in the skin-friction law, and the skin-friction coefficient is obtained by a method presented by Persh. (See ref. 5.) The quantities $\delta^*/\delta$ and $\theta/\delta$ are determined by numerical integration with the use of a real-gas variation of density through the boundary layer. The value of $\theta$ at each point along the nozzle is obtained from the momentum equation by using an iteration scheme, wherein the first approximation to the radial distance is taken to be the sum of the inviscid radial coordinate, at the point of calculation, and the value of $\delta^*$, determined from the previous point of calculation. Successive iterations are made to determine $\delta^*$ within a set accuracy. A detailed description of the method of calculating the displacement thickness is presented in appendix B.

It is the aim of appendices A and B to present the methods of calculation in enough detail to permit one to calculate the coordinates of a hypersonic nozzle directly for the case of a real gas.

## RESULTS AND DISCUSSION

### Inviscid Results

Attention is focused in this section on a number of calculated results which indicate how the various conditions and parameters affect the inviscid nozzle contour. First, a comparison was made between the calculated inviscid contour of a Mach number 17 nozzle based on real-gas properties for nitrogen and the contour based on the ideal-gas properties with a constant heat-capacity ratio of 7/5 for the same stagnation conditions. For this comparison, the stagnation pressure was taken as 1,000 atmospheres and the stagnation temperature was $4{,}200^\circ$ R. The flow properties for the ideal-gas case were taken from reference 6, and for the real-gas case the thermodynamic data of references 7 and 8 were used. This comparison is shown in figure 1, where the throat height for both cases is equal to 0.05 inch. It is noted that the height of the inviscid nozzle exit for the real-gas calculation is approximately 9 percent larger than the exit height based on the ideal-gas calculation. On the other hand, the contour height in the throat region is smaller for the real-gas case than for the corresponding ideal-gas case. This comparison indicates that the inviscid contours for the two cases at the same conditions and Mach number are significantly different, and it appears to be important to include the real-gas effects in hypersonic-nozzle calculations for stagnation conditions in this range.

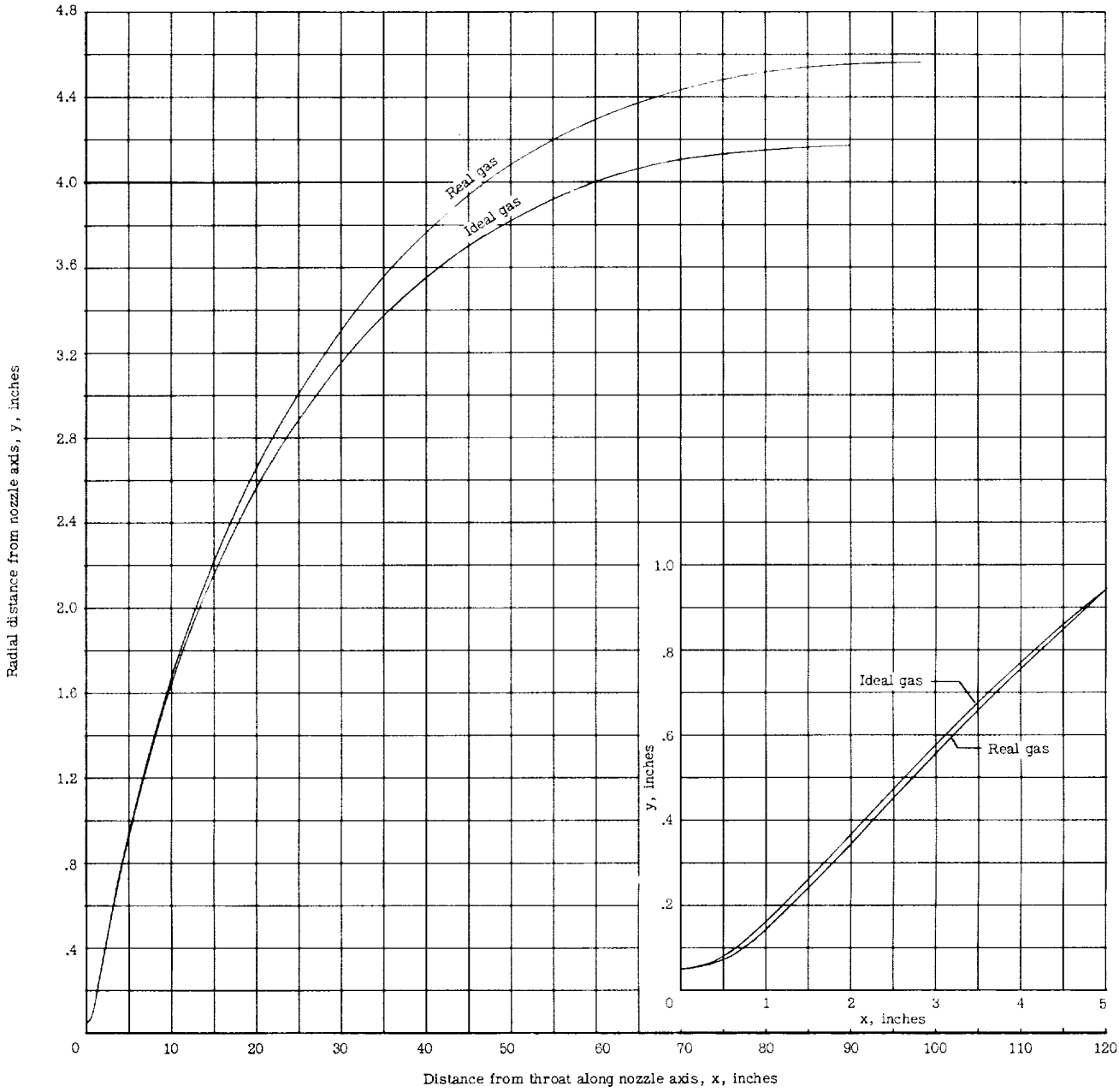


Figure 1.- Comparison of inviscid contour as calculated for a real gas and an ideal gas at $M_1 = 17$, $p_t = 1{,}000$ atmospheres, and $T_t = 4{,}200^\circ$ R.

Two additional inviscid calculations were carried out in order to examine the effect of the choice of stagnation conditions on the inviscid contour of a Mach number 17 nozzle based on real-gas considerations. (It should be noted that the inviscid contour, based on an ideal gas with constant heat capacities, is independent of the stagnation conditions.) The effect of stagnation temperature was examined first. Figure 2 shows the inviscid contours for stagnation temperatures of 4,200° R and 5,000° R, both for a stagnation pressure of 1,000 atmospheres. It is seen that the higher stagnation temperature gives a larger height at the nozzle exit and a decrease in the nozzle contour in the throat region. The effect of stagnation pressure was studied from a comparison of contours calculated for stagnation pressures of 340 atmospheres and 1,000 atmospheres, both at a stagnation temperature of 4,200° R. It is noted from figure 3 that the higher pressure results in a smaller inviscid exit height and a somewhat larger contour height in the throat region.

## Boundary-Layer Results

In addition to the degree to which a nozzle contour is dependent on the real-gas effects in the inviscid region, the boundary-layer displacement thickness can also be influenced by real-gas effects within the boundary layer itself. The calculated boundary-layer displacement thickness will, therefore, be influenced by (1) the real-gas flow properties and their gradients along the edge of the inviscid flow field as determined from the inviscid calculations, and (2) the real-gas properties within the boundary layer.

The degree to which these two effects influence the growth of the displacement thickness for a Mach number 17 nozzle with stagnation conditions of 1,000 atmospheres and 4,200° R with a throat diameter of 0.10 inch was examined by comparison of the growth of $\delta^*$ for three cases: (1) the inviscid flow field is calculated with the use of real-gas properties and the calculations within the boundary layer include the real-gas properties; (2) the inviscid flow field is again calculated with the use of real-gas properties, but the calculations within the boundary layer are based on an ideal gas with a constant heat-capacity ratio of 7/5; and (3) both the inviscid flow and the boundary layer are based on an ideal gas with a constant heat-capacity ratio of 7/5. This comparison is presented in figure 4. It is noted from this figure that the largest difference is between the purely real-gas calculation and the purely ideal-gas result. At an axial distance from the throat of 90 inches, the value of $\delta^*$ for the purely real-gas case is approximately 13 percent larger than for the purely ideal-gas case. On the other hand, figure 4 shows that the value of $\delta^*$ at the same location for a real-gas boundary layer is only about 4 percent larger than that calculated for the ideal-gas boundary layer with a heat-capacity ratio of 7/5, when both results are based on the same real-gas inviscid flow field. Based on these limited calculations, it appears that the real-gas effects in the inviscid flow field have a stronger influence on the determination of the displacement thickness than the real-gas effects within the boundary layer itself.

An attempt was made to see why the displacement thickness is only slightly different for the calculation based on real-gas properties within the boundary

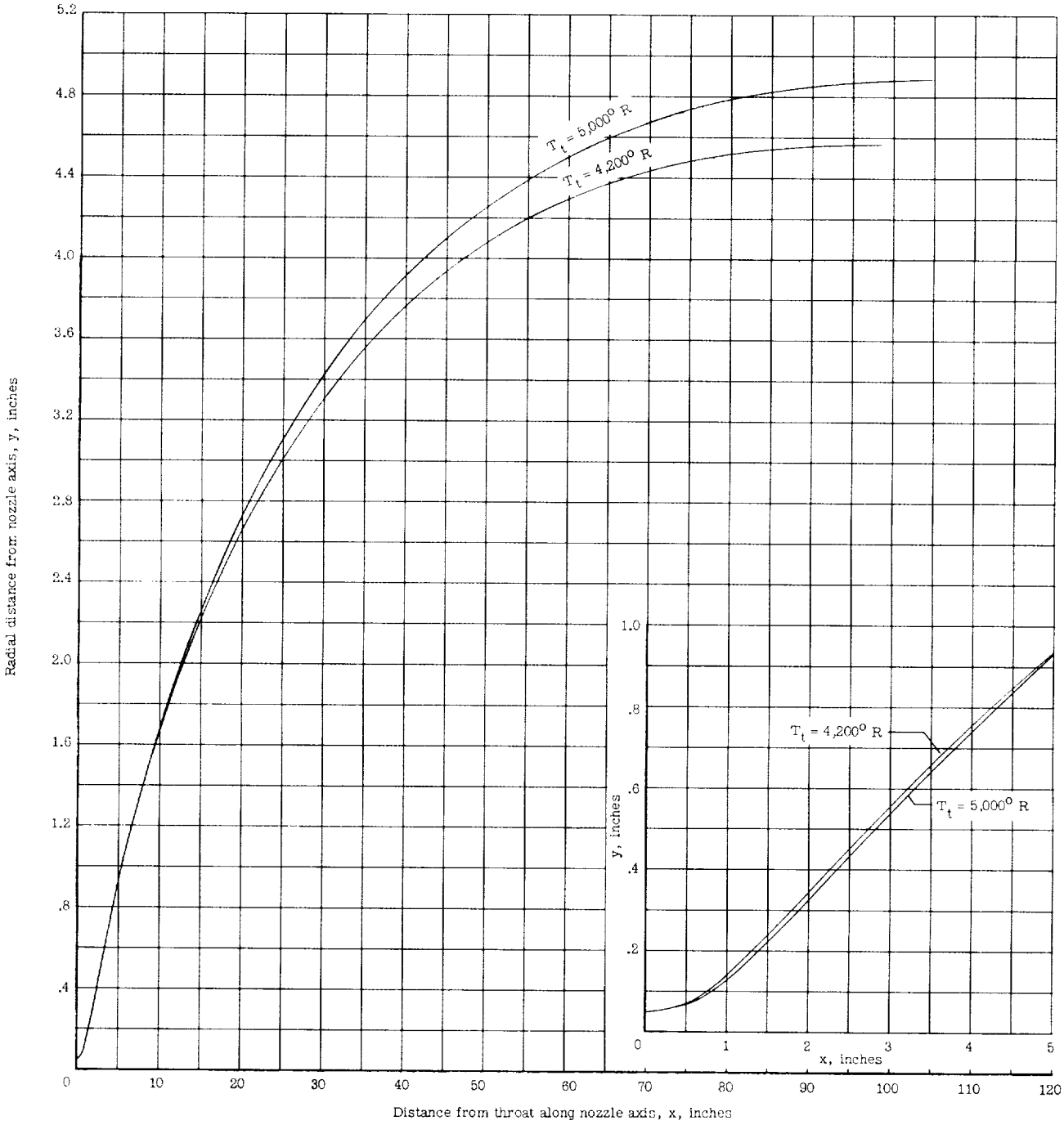


Figure 2.- Effect of stagnation temperature on inviscid nozzle contour as calculated for a real-gas nozzle at $M_1 = 17$ and $p_t = 1{,}000$ atmospheres.

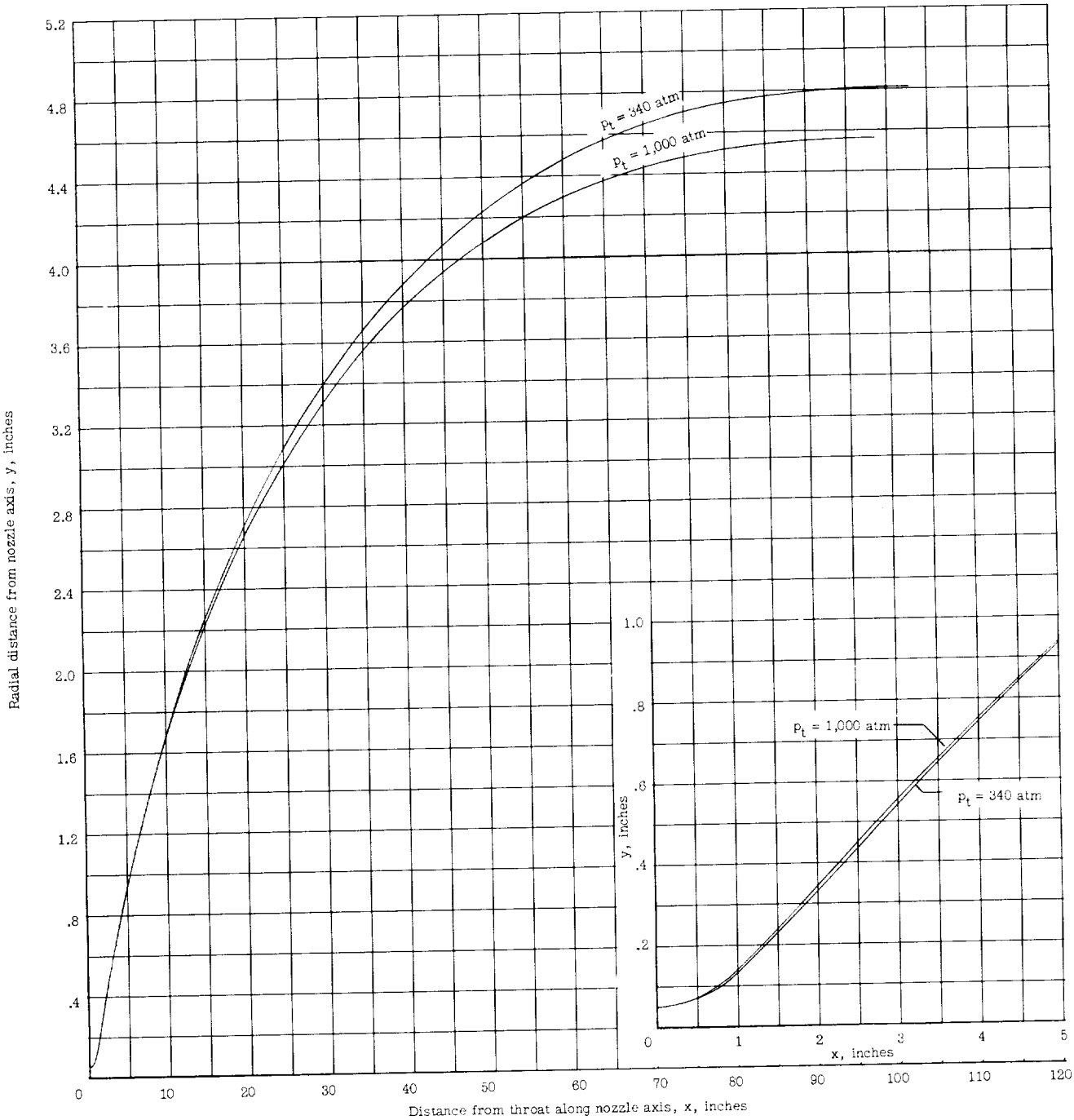


Figure 3.- Effect of stagnation pressure on inviscid nozzle contour as calculated for a real-gas nozzle at $M_1 = 17$ and $T_t = 4{,}200^\circ$ R.


Figure 4.- Growth of boundary-layer displacement thickness as calculated for: (1) a real-gas inviscid contour with a real-gas boundary layer; (2) a real-gas inviscid contour with an ideal-gas boundary layer; and (3) an ideal inviscid contour with an ideal-gas boundary layer. $p_t$ = 1,000 atmospheres; $T_t$ = 4,200° R; $T_w$ = 650° R; d* = 0.10 inch.

layer compared with the case for which ideal-gas properties with constant heat-capacity ratio were used within the boundary layer. The quantity

$$\frac{\frac{7}{2}T}{\frac{7}{2}T + \left(\frac{\Theta}{e^{\Theta/T} - 1}\right)}$$

which represents the ratio of the local static enthalpy, excluding the vibrational component, to the enthalpy including the vibrational mode was calculated across the boundary layer at several positions along the nozzle. The expression for the enthalpy, including the vibrational mode, is presented in reference 9. This quantity is unity when the vibrational component of enthalpy is zero and decreases continuously from unity as the vibrational component becomes more significant.

Figure 5 shows this quantity plotted as a function of the nondimensional distance through the boundary layer $\tilde{y}/\delta$ at longitudinal distances from the nozzle throat of approximately 0.1, 1.0, and 100 inches. These calculations are based on a Mach number 17 nozzle with stagnation conditions of 1,000 atmospheres and stagnation temperature of 4,200° R and with a wall temperature of 650° R. It can be seen from figure 5 that the vibrational component of the local static enthalpy is always less than 10 percent of the total local static enthalpy $\frac{7}{2}T + \left(\frac{\Theta}{e^{\Theta/T} - 1}\right)$ at any position within the boundary layer, even very near the nozzle throat. At a distance of 1 inch downstream from the throat, the enthalpy in the vibrational mode is less than 4 percent of the local static enthalpy and further downstream becomes even less significant. Because there is only a small percentage of the local static enthalpy at each point within the boundary layer in the vibrational mode, the small effect noted between the real-gas and ideal-gas boundary-layer results should be expected. The effect of pressure on the local static enthalpy within the boundary layer for the conditions of this example were found to be very small so that essentially all of the real-gas effects within the boundary layer are due to the vibrational component of enthalpy.

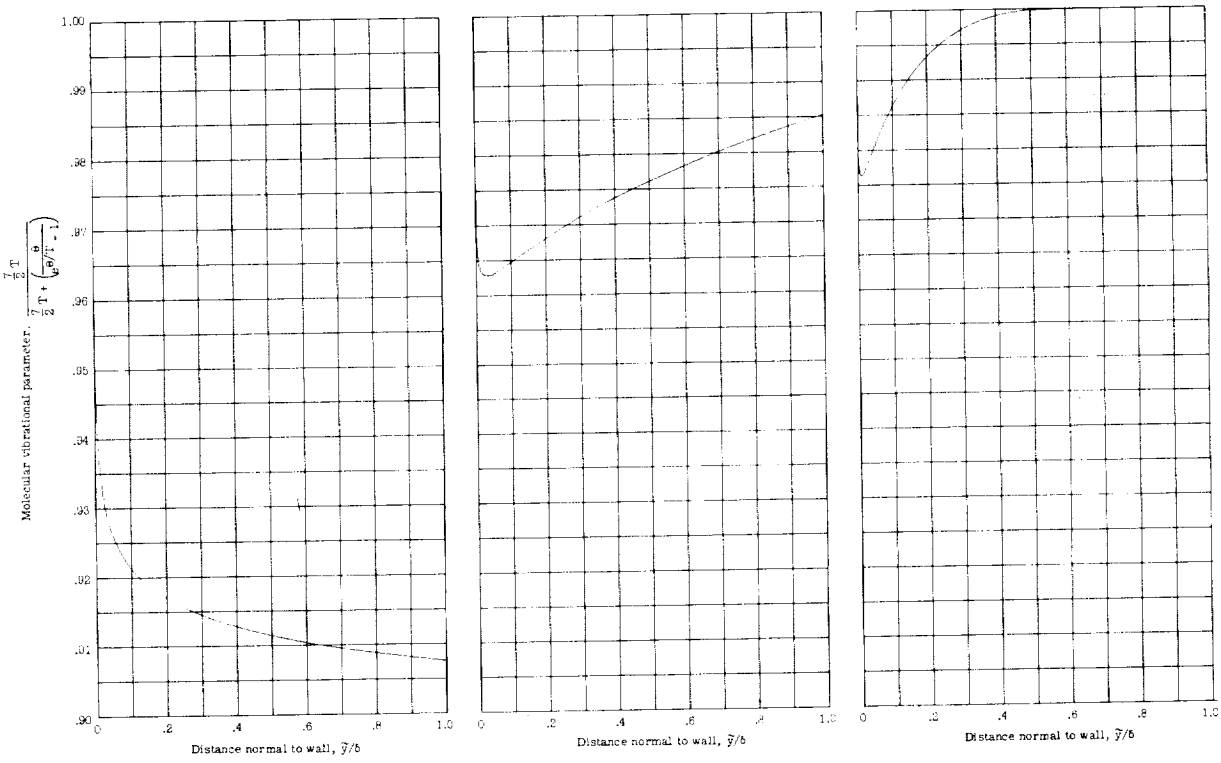


(a) x = 0.1 inch. (b) x = 1.0 inch. (c) x = 100 inches.

Figure 5.- Effect of molecular vibration on enthalpy through boundary layer at three locations of x as calculated for a real-gas nozzle at $M_1 = 17$, $p_t = 1{,}000$ atmospheres, $T_t = 4{,}200°$ R, $T_w = 650°$ R, and $d^* = 0.10$ inch.

In figure 6, a comparison of the calculated displacement thickness similar to that presented in figure 4 is given, the only difference being that the stagnation temperature for the results shown in figure 6 is 5,000° R. The comparison shown in figure 6 for 5,000° R is qualitatively the same as that shown in figure 4 for 4,200° R. The comparison presented in figure 6 indicates, however, that the higher stagnation temperature results in a greater difference between the displacement thickness based on real-gas properties in the boundary layer as compared to those based on ideal-gas properties. This greater difference is believed to be due to the larger percentage of the local static enthalpy in the vibrational mode within the boundary layer at higher temperatures.

In order to obtain an indication of the effect of stagnation conditions on the growth of the displacement thickness in a Mach number 17 nozzle, two sets of

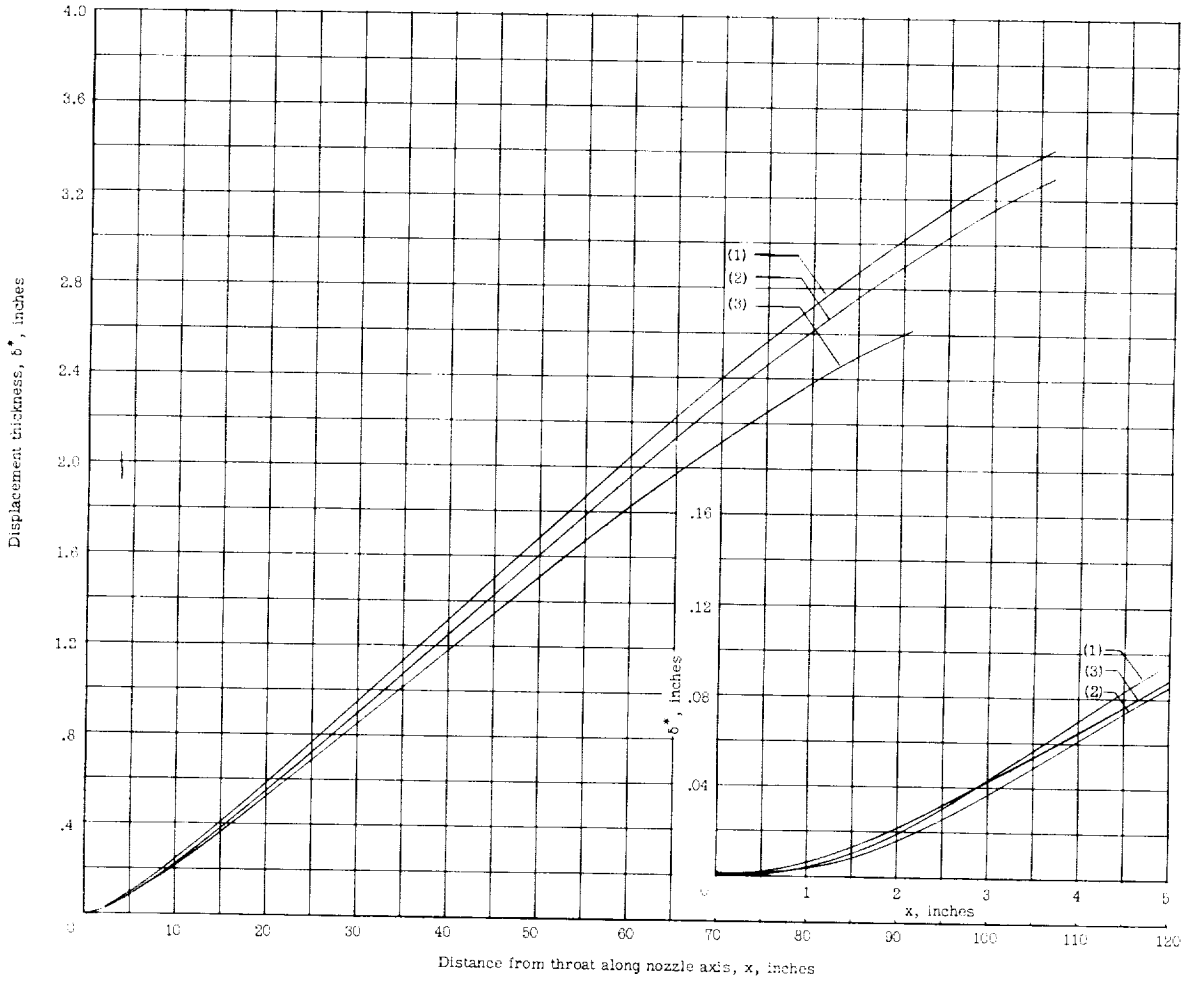


Figure 6.- Growth of boundary-layer displacement thickness as calculated for: (1) a real-gas inviscid contour with a real-gas boundary layer; (2) a real-gas inviscid contour with an ideal-gas boundary layer; and (3) an ideal inviscid contour with an ideal-gas boundary layer. $p_t$ = 1,000 atmospheres; $T_t$ = 5,000° R; $T_w$ = 650° R; and $d^*$ = 0.10 inch.

calculations were made. In the first set, the stagnation pressure was chosen to be 1,000 atmospheres, and the stagnation temperature was set equal to 4,200° R and 5,000° R. For the second set of calculations, the stagnation temperature was chosen to be 4,200° R and the stagnation pressure was set equal to 340 atmospheres and 1,000 atmospheres. The results of these two sets of calculations are presented in figures 7 and 8. It can be seen that an increase in stagnation temperature or a decrease in stagnation pressure results in a larger displacement thickness at each position along the nozzle. It should be remembered that these calculations of $\delta^*$ are also influenced by the changes in the inviscid flow field due to changes in stagnation conditions.

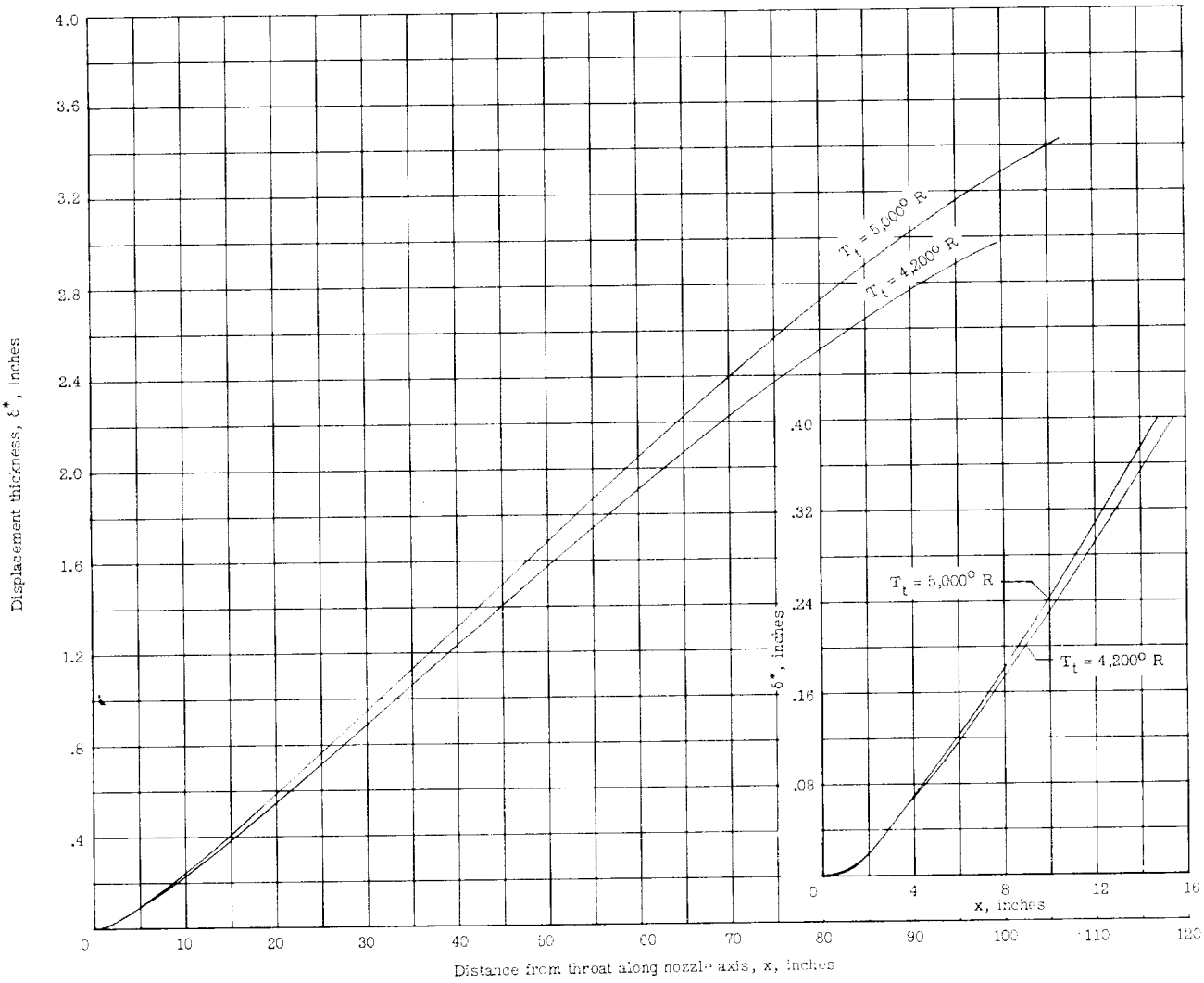


Figure 7.- Effect of stagnation temperature on growth of real-gas boundary-layer displacement thickness as calculated for a real-gas nozzle at $M_1 = 17$, $p_t$ = 1,000 atmospheres, $T_w = 650°$ R, and $d^* = 0.10$ inch.

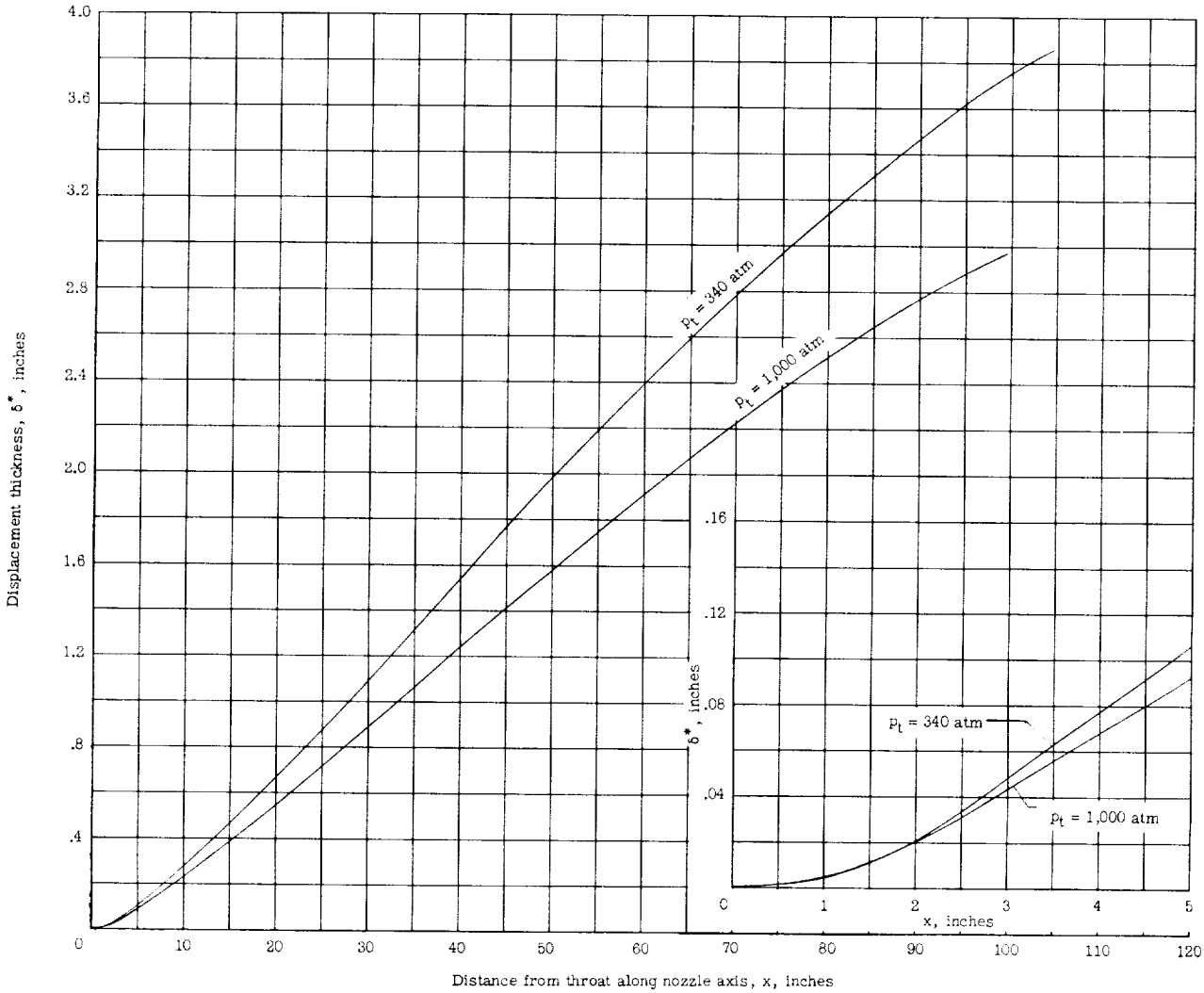


Figure 8.- Effect of stagnation pressure on growth of real-gas boundary-layer displacement as calculated for a real-gas nozzle at $M_1 = 17$, $T_t = 4{,}200^\circ$ R, $T_w = 650^\circ$ R, and $d^* = 0.10$ inch.

Because the physical-wall contour is the ultimate objective in the calculation of a nozzle, figure 9 was prepared to show the difference between the physical-wall contours based on real-gas properties and on properties based on ideal gas with constant heat-capacity ratio of 7/5. This comparison is for a Mach number 17 nozzle with stagnation conditions of 1,000 atmospheres and $4{,}200^\circ$ R. It can be seen that the contour based on the ideal gas with constant heat-capacity ratio is significantly different from that based on the real-gas properties.

The calculated values of $\delta^*$ along the nozzle are based on a method that requires a number of assumptions which lead to limited certainty as to the correct local displacement thickness. Inasmuch as the physical contour is directly dependent on the calculated values of $\delta^*$, this same absolute uncertainty exists at each location along the physical contour. It should be noted, however, that

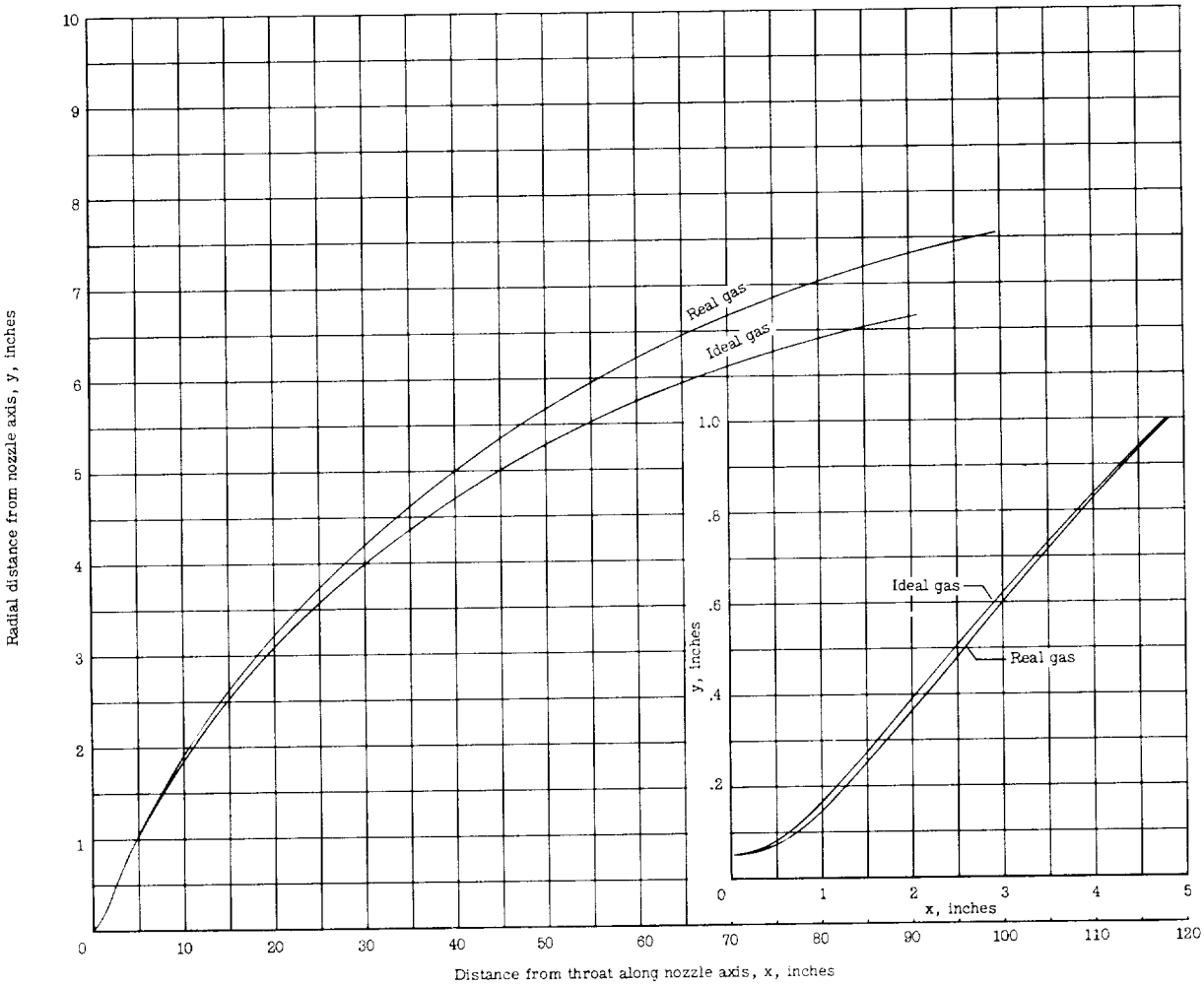


Figure 9.- Comparison of wall contour as calculated for an ideal-gas nozzle (ideal inviscid and ideal boundary layer) and a real-gas nozzle (real inviscid and real boundary layer) at $M_1 = 17$, $p_t = 1{,}000$ atmospheres, $T_t = 4{,}200^\circ$ R, $T_w = 650^\circ$ R, and $d^* = 0.10$ inch.

the absolute values of $\delta^*$ are rather small in the throat region so that the physical contour in the throat region is essentially determined only by the inviscid calculations. Further downstream, however, the boundary layer becomes a significant fraction of the physical contour.

Effect of nozzle wall temperature.- The results of calculations presented up to this point are based on a constant wall temperature of 650° R. The effect of wall temperature on the calculated values of $\delta^*$ was examined by comparison of results based on constant wall temperatures of 650° R and 1,500° R for a Mach number 17 nozzle with stagnation conditions of 1,000 atmospheres and 4,200° R. This comparison is presented in figure 10. It can be seen that an increase in wall temperature from 650° R to 1,500° R causes only a slight decrease in the displacement thickness along the nozzle. At the nozzle exit the difference is less than 1.0 percent, whereas, in the throat region the displacement thickness

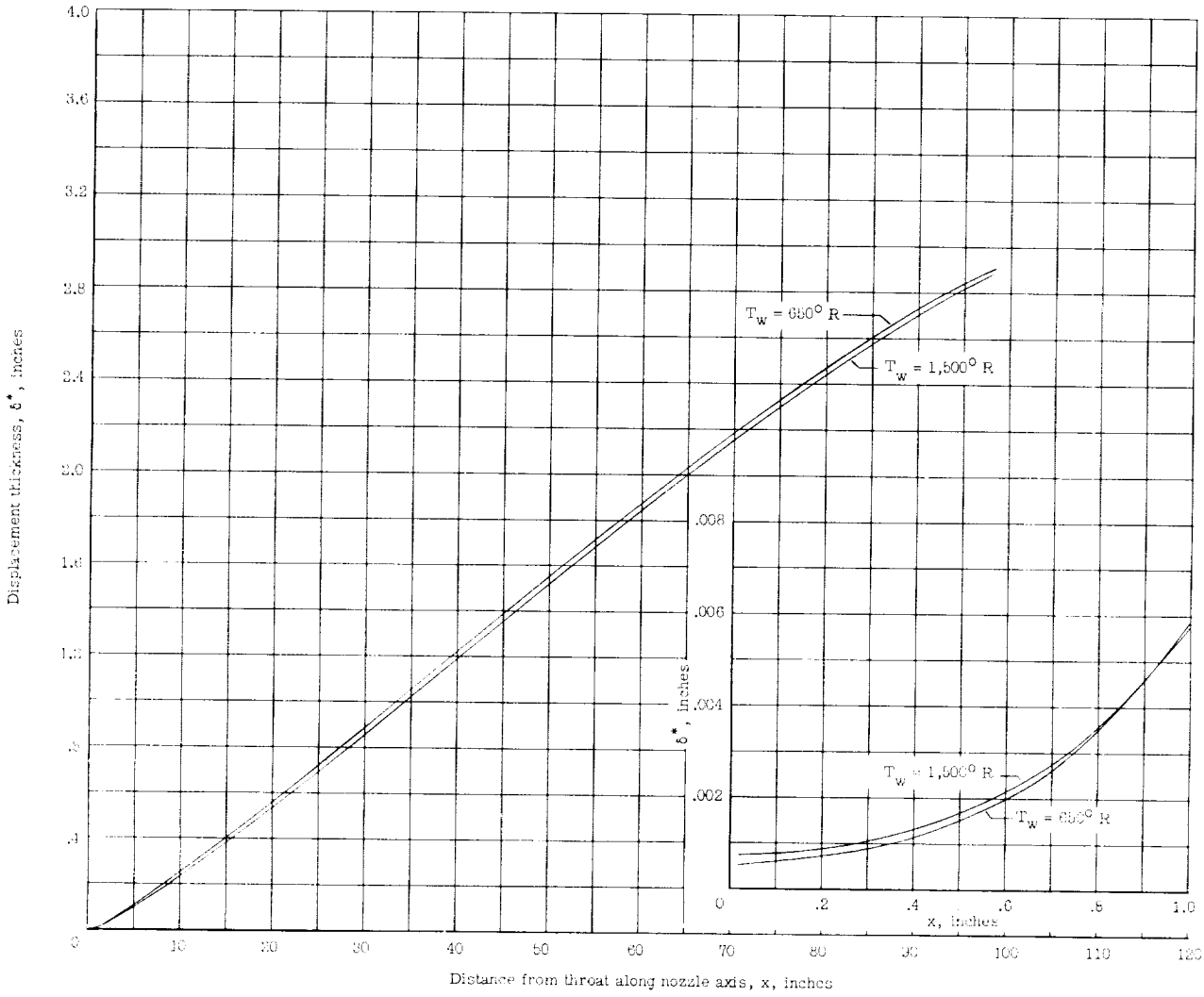


Figure 10.- Effect of wall temperature on growth of boundary-layer displacement thickness as calculated for a real-gas nozzle at $M_1 = 17$, $p_t = 1{,}000$ atmospheres, $T_t = 4{,}200^\circ$ R, and $d^* = 0.10$ inch.

for the wall temperature of 650° R was less than 0.0002 inch smaller than the case for 1,500° R. Based on this calculation, the wall temperature does not affect the displacement thickness to a large extent.

The results show that the displacement thickness was only slightly affected by a change in wall temperature from 650° R to 1,500° R; the boundary-layer profiles of mass flow per unit area $\rho u'/\rho_1 u_1$ and $\rho/\rho_1$ for these two temperatures at 0.1, 1.0, and 100 inches from the throat were calculated as well as values of $\delta^*/\delta$, $\theta/\delta$, and $\theta$ at the same nozzle positions. The profiles are presented in figures 11, 12, and 13, and the corresponding values of $\delta^*/\delta$, $\theta/\delta$, and $\theta$ are shown in table I. It is noted from these three figures that profiles for both wall temperatures change appreciably along the nozzle but are qualitatively the same for both wall temperatures at a given nozzle position. The tabulated results of table I show that $\delta^*/\theta$ increases with wall temperature, but there

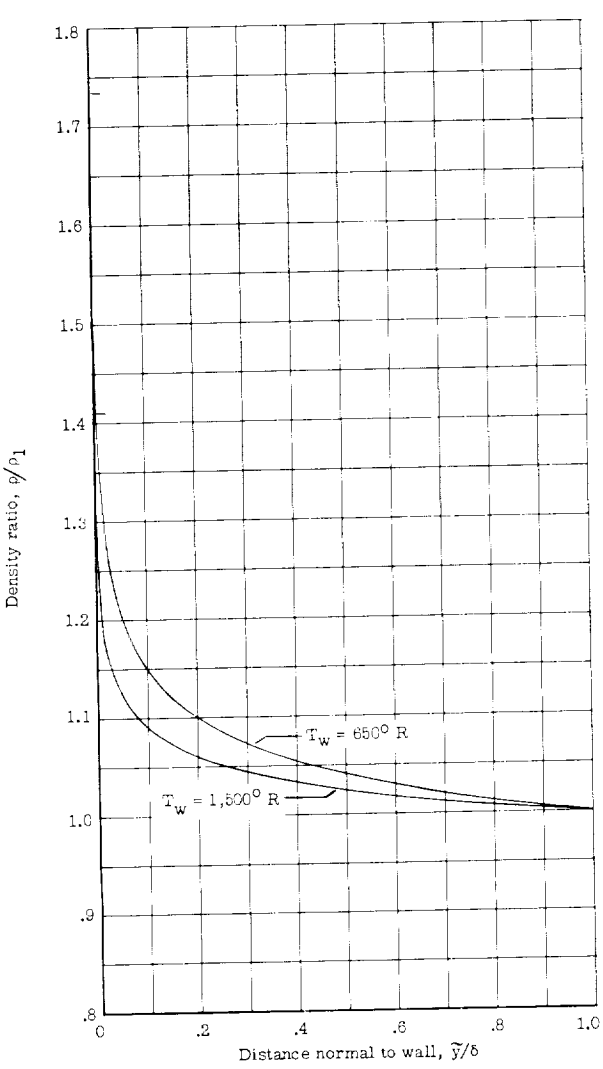


(a) Density ratio.

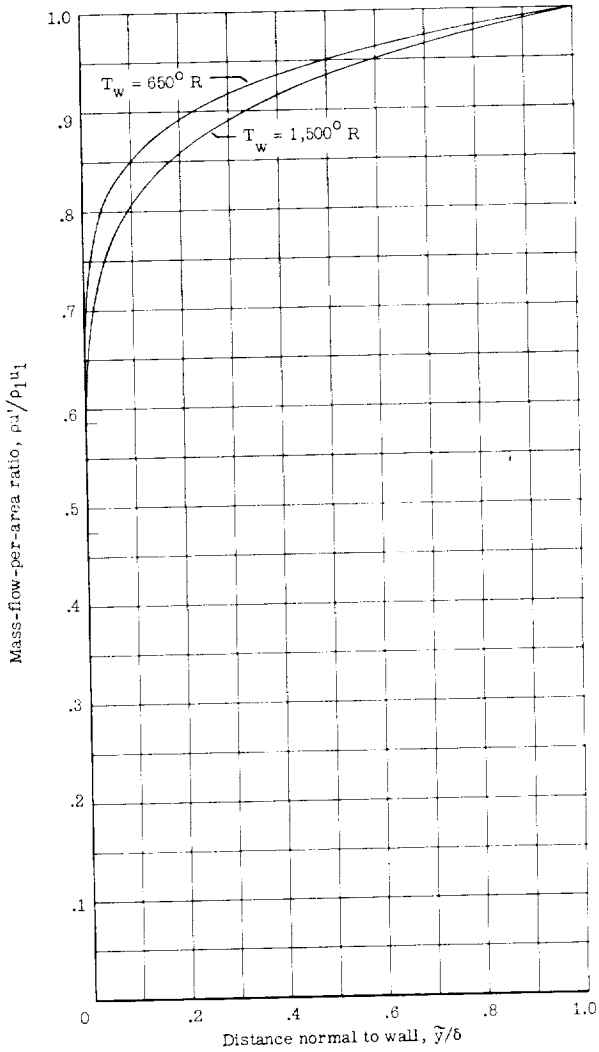


(b) Mass rate of flow per area.

Figure 11.- Boundary-layer profiles of density ratio and ratio of mass flow per area as calculated for wall temperatures of 650° R and 1,500° R at $x$ = 0.1 inch, $p_t$ = 1,000 atmospheres, $T_t$ = 4,200° R, N = 7.58, and $d^*$ = 0.10 inch.

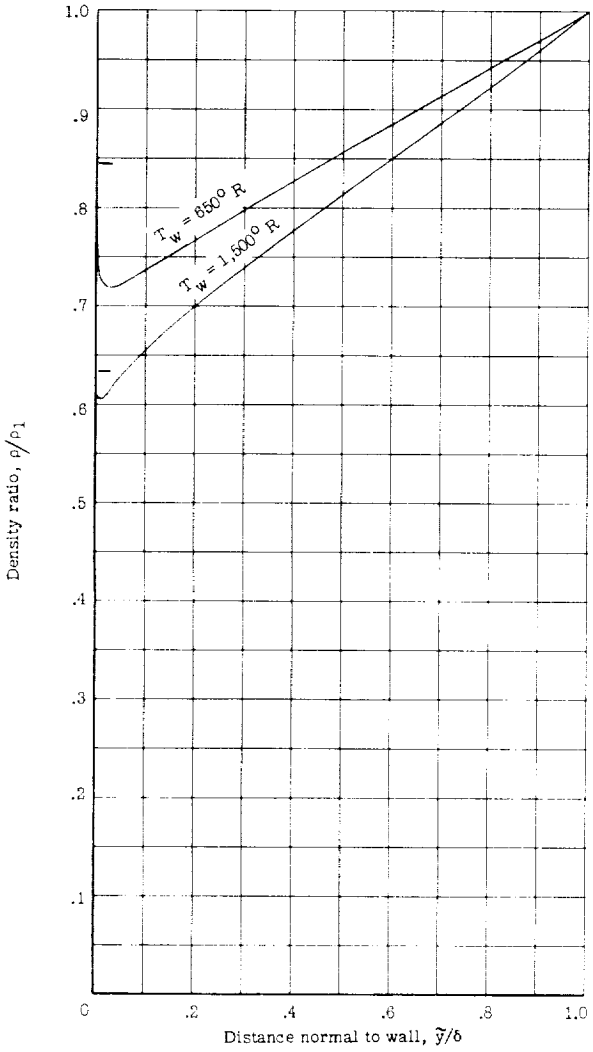


(a) Density ratio.

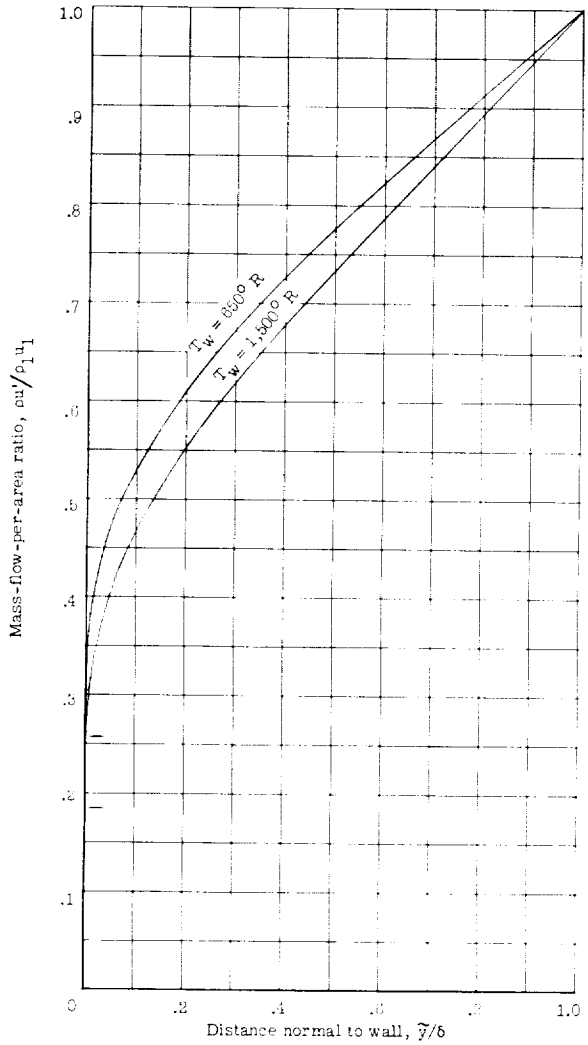


(b) Mass rate of flow per area.

Figure 12.- Boundary-layer profiles of density ratio and ratio of mass flow per area as calculated for wall temperatures of 650° R and 1,500° R at $x = 1.0$ inch, $p_t = 1,000$ atmospheres, $T_t = 4,200^\circ$ R, $N = 6.93$, and $d^* = 0.10$ inch.

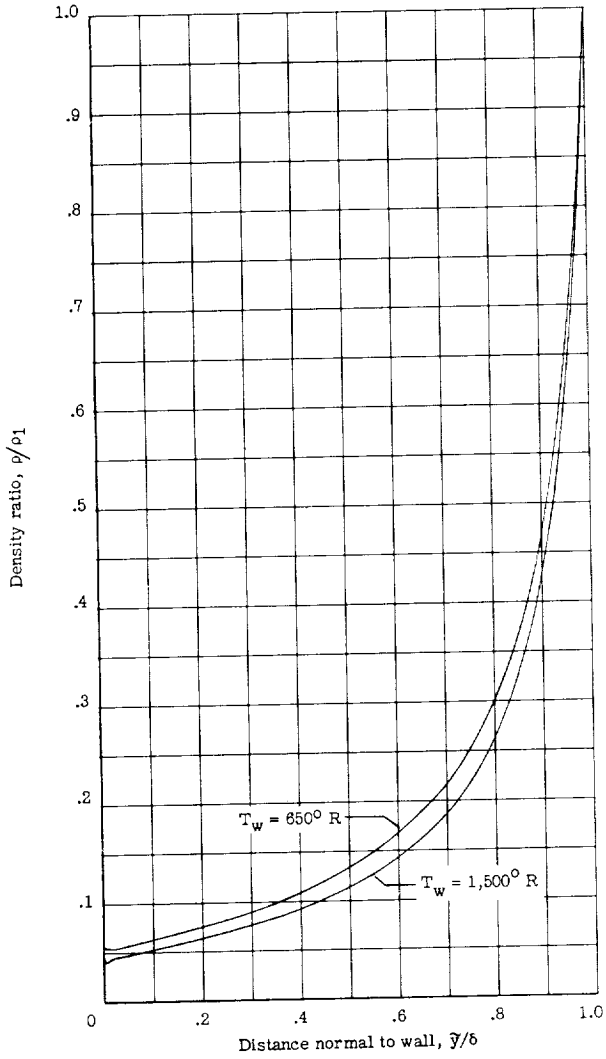


(a) Density ratio.

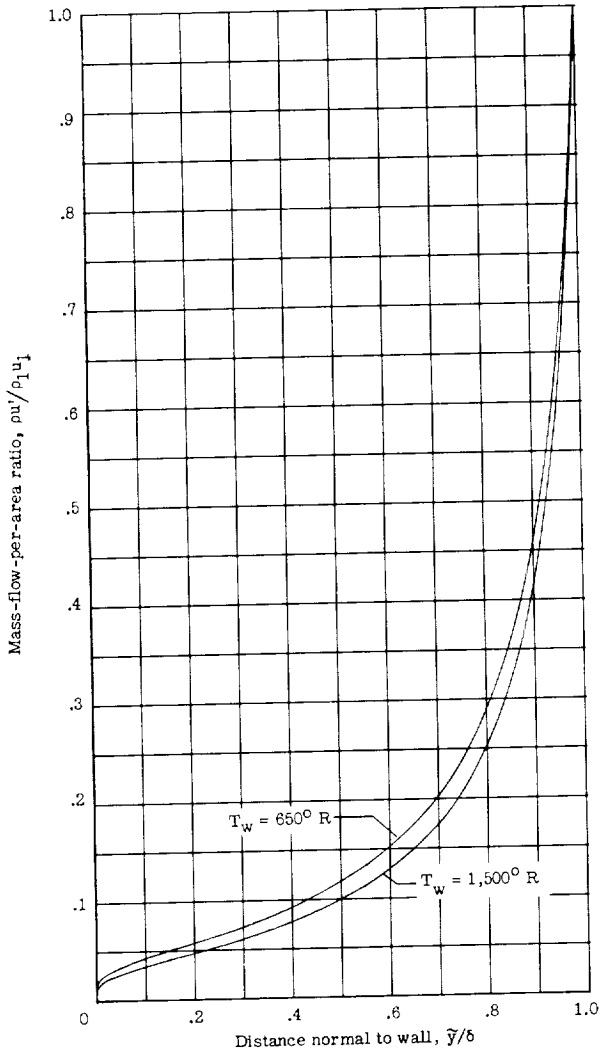


(b) Mass rate of flow per area.

Figure 13.- Boundary-layer profiles of density ratio and ratio of mass flow per area as calculated for wall temperatures of 650° R and 1,500° R at $x = 100$ inches, $p_t = 1{,}000$ atmospheres, $T_t = 4{,}200°$ R, $N = 5.83$, and $d^* = 0.10$ inch.

TABLE I

BOUNDARY-LAYER PARAMETERS FOR A MACH NUMBER 17 NOZZLE AT

$p_{t,1}$ = 1,000 ATMOSPHERES AND $T_{t,1}$ = 4,200° R

| x, in. (approx.) | $T_w$, °R | $\frac{\delta^*}{\delta}$ | $\frac{\theta}{\delta}$ | $\frac{\delta^*}{\theta}$ | $\theta$, in. |
|---|---|---|---|---|---|
| 0.1 | 650<br>1,500 | 0.065<br>.085 | 0.103<br>.099 | 0.63<br>.86 | 0.00095<br>.00090 |
| 1.0 | 650<br>1,500 | 0.24<br>.28 | 0.079<br>.074 | 3.00<br>3.74 | 0.0020<br>.0016 |
| 100 | 650<br>1,500 | 0.81<br>.83 | 0.012<br>.011 | 66.80<br>79.00 | 0.044<br>.036 |

is also a simultaneous decrease in $\theta$ which is assumed to be caused by a corresponding change in the value of $C_f/2$ determined from the skin-friction relation. The two effects tend to make $\delta^*$ insensitive to wall temperature.

The results of the work presented in reference 2 indicate that the choice of the skin-friction relation which is used in the boundary-layer calculation has an effect on the resulting values of $\delta^*$. It is shown in reference 2 that a change in wall temperature from 583° R to 1,500° R resulted in an increase in $\delta^*$ when one skin-friction relation was used, whereas another skin-friction relation indicated a decrease in $\delta^*$ for the same temperature change.

The skin-friction law of Persh (ref. 5) was selected for this present work based on satisfactory calibration results presented in reference 10. The nozzles tested in reference 10 showed good agreement with the designed performance based on Persh's skin-friction relation for the calculation of the displacement thickness.

In order that the nozzle wall temperature be more realistic in the actual nozzle operating conditions, a variable wall temperature was assumed along the nozzle with a hot wall in the throat region and a cooler wall downstream. The three wall-temperature variations which were used are plotted in figure 14 and are labeled (a), (b), and (c). Each of these temperature distributions begins at the nozzle throat with a temperature of 2,820° R and decreases continuously according to the equation indicated on the figure to asymptotic values for curves (a), (b), and (c) of 2,350° R, 1,500° R, and 650° R, respectively, further downstream. These wall-temperature variations are discussed in more detail in appendix B. The effect which these three wall-temperature variations have on the

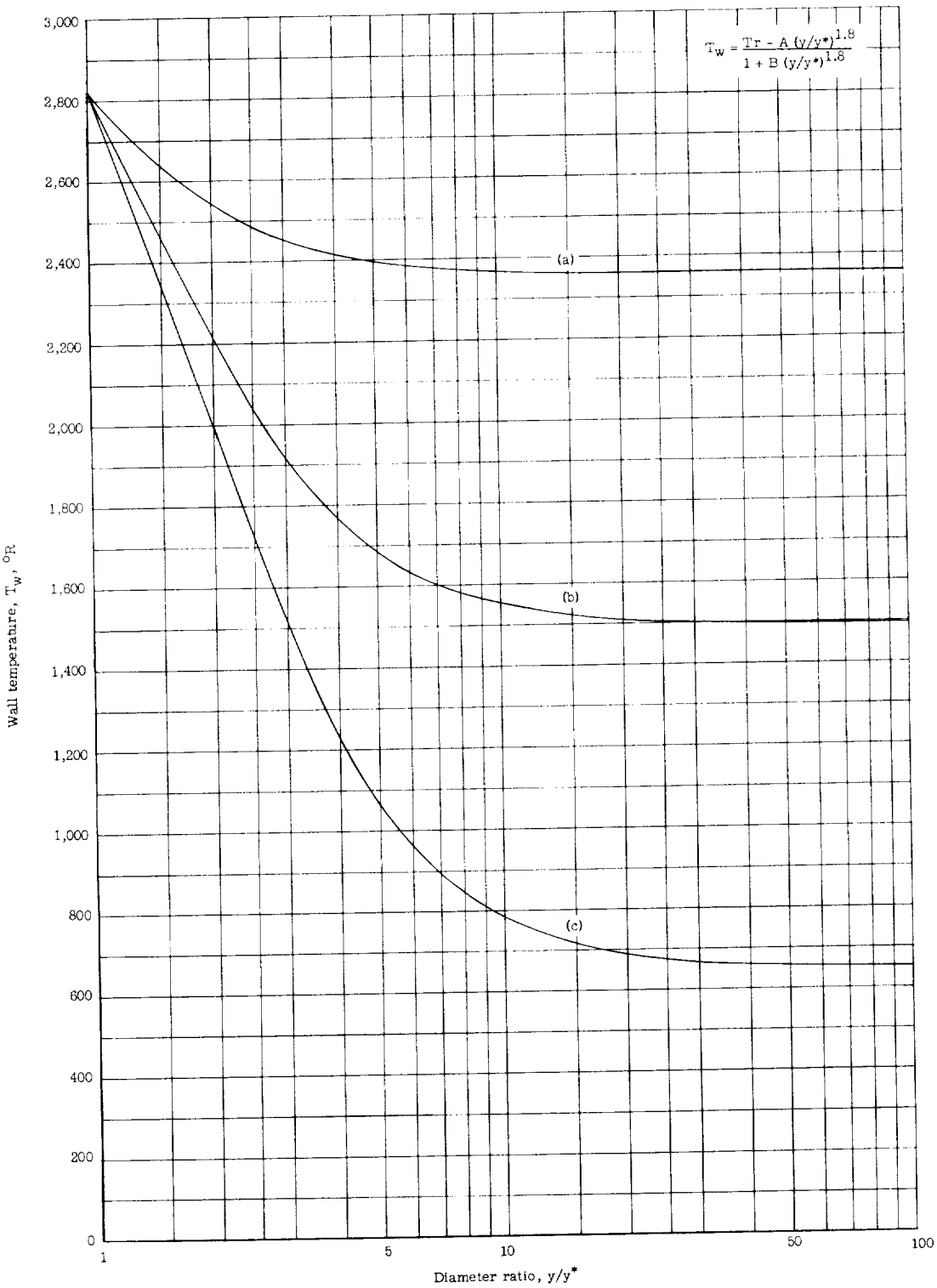


Figure 14.- Assumed variations of wall temperature with diameter ratio.

calculated displacement thickness along a nozzle is shown in figure 15. It is

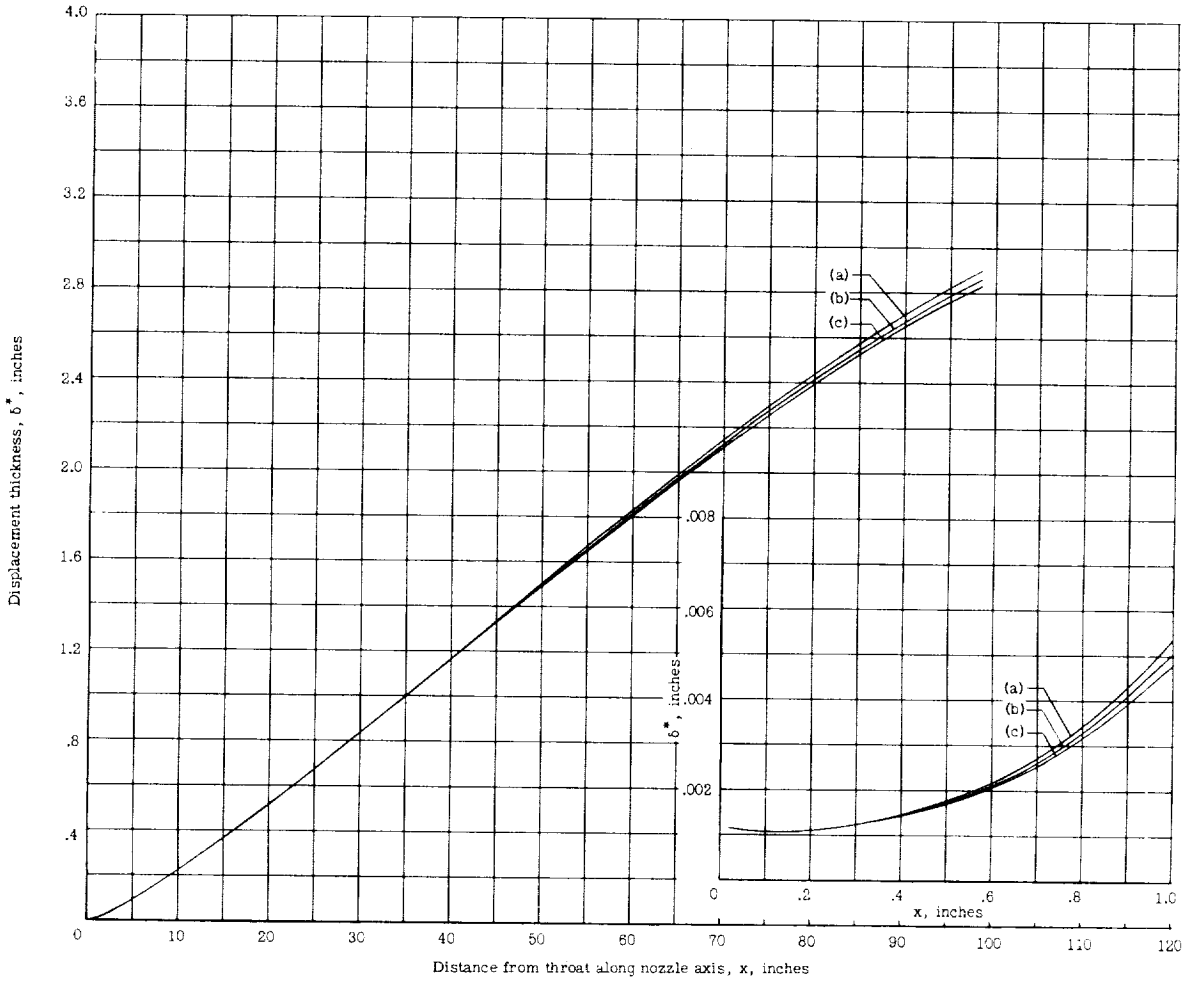


Figure 15.- Effect of variable wall temperatures on growth of boundary-layer displacement thickness as calculated for a real-gas nozzle at $M_1 = 17$, $p_t = 1{,}000$ atmospheres, $T_t = 4{,}200^\circ$ R, and $d^* = 0.10$ inch. (See fig. 14 for wall temperatures.)

noted that the displacement thickness is only slightly influenced by the wall temperature. The reason for realizing only a small effect is believed to be due to the opposing changes in $\delta^*/\theta$ and $\theta$ with a change in wall temperature as discussed before.

Effect of pressure on enthalpy.- As mentioned before, the real-gas effects considered in this work include the deviations from ideal-gas behavior due to excitation of the vibrational energy modes and to the high-density or high-pressure effects. Both of these effects are accounted for in the calculation of the inviscid flow field by use of the real-gas properties of nitrogen. In the

boundary-layer calculations, however, the vibrational effect on enthalpy is accounted for by an analytical expression with a function only of temperature. This analytical expression is then multiplied by a correction term which is the ratio of the actual enthalpy, including pressure effects, divided by the enthalpy based on the temperature alone. This pressure-correction term for the enthalpy is denoted as $Q$ and is of the order of unity. The application of this correction term is discussed in appendix B. The influence which the real-gas effects due to high pressure alone have on the calculation of $\delta^*$ is shown in figure 16 for a particular nozzle in the region near the throat. It can be seen that the difference between the result when using $Q$ equal to unity (that is, no real-gas pressure effect considered) and the result when $Q$ was taken into account, is at most a few percent for the conditions of this calculation. For higher stagnation pressures at the same temperature or for lower stagnation temperatures at the same pressure, that is, higher densities, the influence of using the actual values of $Q$ would be greater.

## Computer Program

The calculated results were obtained by use of an IBM 7090 electronic data processing system at the Langley Research Center. A listing of the detailed program statements in FORTRAN language (ref. 11) are presented in appendix C with appropriate comments for the benefit of agencies having access to digital computing machines. This program was set up and used to calculate hypersonic nozzle contours with nitrogen for stagnation temperatures up to $5{,}000^\circ$ R and stagnation pressures up to 1,000 atmospheres. It should be pointed out that the method for calculating the inviscid flow field is general and can also be applied directly to other gases for stagnation conditions such that equilibrium dissociation effects must be considered. This method can, of course, also be applied to the calculation of the inviscid region of a hypersonic nozzle using helium at high stagnation pressures, for which case real-gas effects due to high density can be quite significant. The inputs to this present program for such cases would be the same as used in this work for the inviscid region, namely, the real-gas relation between the Mach number and limiting-velocity ratio and the relation between the ratio of free-stream to stagnation density, and the limiting-velocity ratio for an isentropic expansion from a given stagnation condition.

That part of the program which is concerned with the calculation of the boundary-layer displacement thickness, however, would in general require some modifications for other gases and much different stagnation conditions considered herein. A relation between the local static enthalpy within the boundary layer and the local pressure and temperature would be required which would replace equations (B9) of appendix B. Accordingly, this would change the form of equation (B12). The skin-friction law given by equations (B13), (B14), and (B15), could also be replaced by another law, if desired, or modified for a particular case.

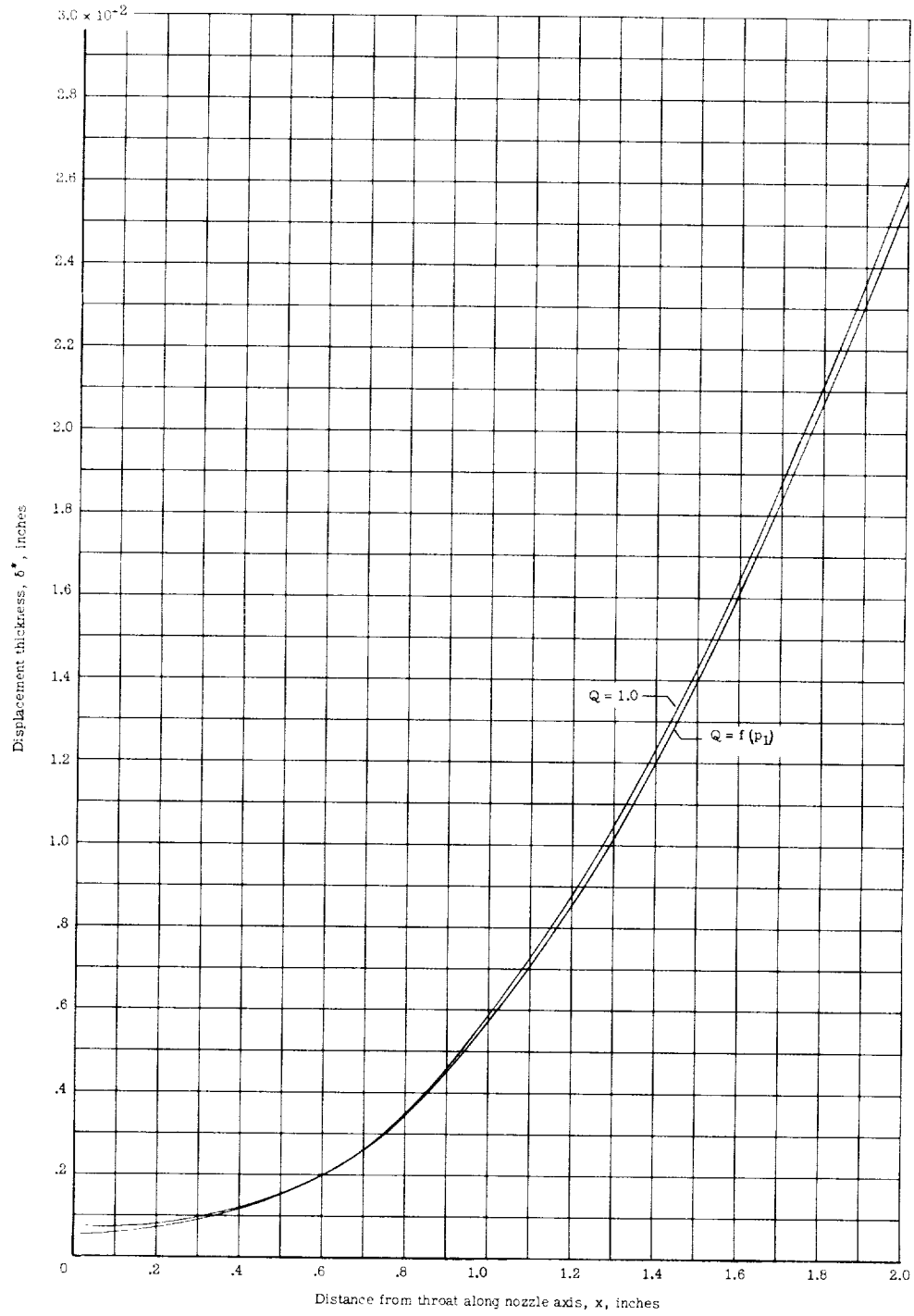


Figure 16.- Effect of Q on growth of boundary-layer displacement thickness as calculated at $M_1 = 17$, $p_t = 1{,}000$ atmospheres, $T_t = 4{,}200^\circ$ R, $T_w = 650^\circ$ R, and $d^* = 0.10$ inch.

## CONCLUDING REMARKS

A method for calculating a hypersonic-nozzle contour for a real gas has been developed and incorporated into a computer program which facilitates the rapid calculation of the inviscid flow field and the wall-boundary-layer displacement thickness. The procedure for calculating both the inviscid region and the displacement thickness is presented in enough detail to permit the direct application of this method. A working FORTRAN program for use on an IBM 7090 electronic data processing system is also presented.

The inviscid contour and the corresponding displacement thickness have been calculated for a number of conditions for nitrogen with stagnation temperatures up to 5,000° R and stagnation pressures up to 1,000 atmospheres for a Mach number of 17. The real-gas effects considered in these calculations are those that are associated with high-density gases and the variation of heat capacity with temperature due to vibrational excitation. This method of calculation presented herein may be applied to a number of systems with some modifications. Rather simple modifications are required for the consideration of equilibrium dissociated flow.

Based on a number of calculations and the use of the present method, the following conclusions are indicated:

1. A comparison between a calculated inviscid contour of a Mach number 17 nozzle based on real-gas properties for nitrogen and on ideal-gas relations with a constant heat-capacity ratio of 7/5 for stagnation conditions of 1,000 atmospheres and 4,200° R shows that the inviscid contour based on real-gas considerations is considerably different from that found for the ideal gas. For this case, the exit diameter of the inviscid nozzle is approximately 9-percent larger for the real-gas calculation than for the results based on ideal-gas relations. On the other hand, the diameter in the region near the throat is less for the inviscid real-gas result than for the ideal-gas result.

2. It was found that when real-gas effects are taken into account the choice of stagnation conditions strongly affected the inviscid nozzle contour for the conditions examined.

3. The effect of stagnation conditions on the boundary-layer calculations, including real-gas effects, exhibited the same trends as for an ideal gas in that a decrease in the stagnation temperature or an increase in the stagnation pressure resulted in a decrease in the displacement thickness along the nozzle contour.

4. The influence of the real-gas effects within the boundary layer on the calculation of the displacement thickness was much less significant than the influence of real-gas effects in the inviscid flow field on the determination of the inviscid nozzle contour.

5. The calculated displacement thickness for the condition of constant wall temperature was found to be only weakly affected by the level of the wall

temperature. For example, the displacement thickness, calculated for a Mach number 17 nozzle with stagnation conditions of 1,000 atmospheres and 4,200° R and throat diameter of 0.10 inch, based on a wall temperature of 650° R was less than 1 percent greater than the value for a wall temperature of 1,500° R at the nozzle exit. In the throat region the displacement thickness for the case in which the wall temperature was 650° R was less than 0.0002 inch smaller than the case for 1,500° R. Also, calculations in which several realistic wall-temperature variations along the nozzle contour were assumed indicated that the wall-temperature level and its variation along the nozzle do not strongly affect the calculated displacement thickness for the method presented herein.

Langley Research Center,
National Aeronautics and Space Administration,
Langley Station, Hampton, Va., January 7, 1963.

## APPENDIX A

## CALCULATION OF INVISCID NOZZLE CONTOUR FOR A REAL GAS

### Characteristic Equations

The procedure for calculating the inviscid nozzle contour for air as a real gas was briefly discussed in reference 3. The approach used in this present work is essentially the same for the inviscid calculations. The basic equation for determining the inviscid contour for an axially symmetric nozzle is the potential-flow equation presented in reference 12 (p. 261, eq. (469)). The solution to this equation can be obtained through the method of characteristics which reduces to four characteristic equations which are readily adaptable to a finite difference technique. The derivation of the characteristic equations is also presented in reference 12. These four characteristic equations are:

$$\left.\begin{aligned} \frac{dy}{dx} &= \tan(\mu + \theta) \\ \frac{dW}{W} - d\theta \tan\mu - l_1 \frac{dx}{y} &= 0 \end{aligned}\right\} \text{first family} \qquad \text{(A1)}$$

and

$$\left.\begin{aligned} \frac{dy}{dx} &= \tan(\theta - \mu) \\ \frac{dW}{W} + d\theta \tan\mu - l_2 \frac{dx}{y} &= 0 \end{aligned}\right\} \text{second family} \qquad \text{(A2)}$$

where

$$l_1 = \frac{\sin\mu \sin\theta \tan\mu}{\cos(\mu + \theta)}$$

and

$$l_2 = \frac{\sin\mu \sin\theta \tan\mu}{\cos(\theta - \mu)}$$

These characteristic equations involve the five variables W, $\theta$, x, y, and $\mu$, so that an additional relation is required. For the case of an ideal gas with a

constant specific-heat ratio, the expression relating $M$ to $W$ is

$$\frac{1}{W^2} = 1 + \left(\frac{2}{\gamma - 1}\right)\frac{1}{M^2} \tag{A3}$$

and may be used because $\mu$ is directly related to $M$ by the equation

$$\mu = \sin^{-1}\frac{1}{M} \tag{A4}$$

The equivalent real-gas relation between $W$ and $M$ is obtained by taking the form of the ideal-gas expression as given in equation (A3) and tabulating the quantity $1/W^2$ for various values of $1/M^2$ as calculated for the isentropic expansion from a given stagnation condition. These are the values of $1/W^2$ and $1/M^2$ based on a real gas and are used directly in the calculation procedure with linear interpolation between the tabulated values.

## Determination of Flow Properties Along Flow-Region Boundaries

The two families of characteristic equations (eqs. (A1) and (A2)) are solved by a stepwise procedure in which the initial values of the flow properties $W$, $\theta$, $\bar{x}/r_{cr}$, $y/r_{cr}$, and $M$ are first calculated along the edge of the characteristic flow fields. These initial flow properties are calculated along the line ABCDE of sketch (a).

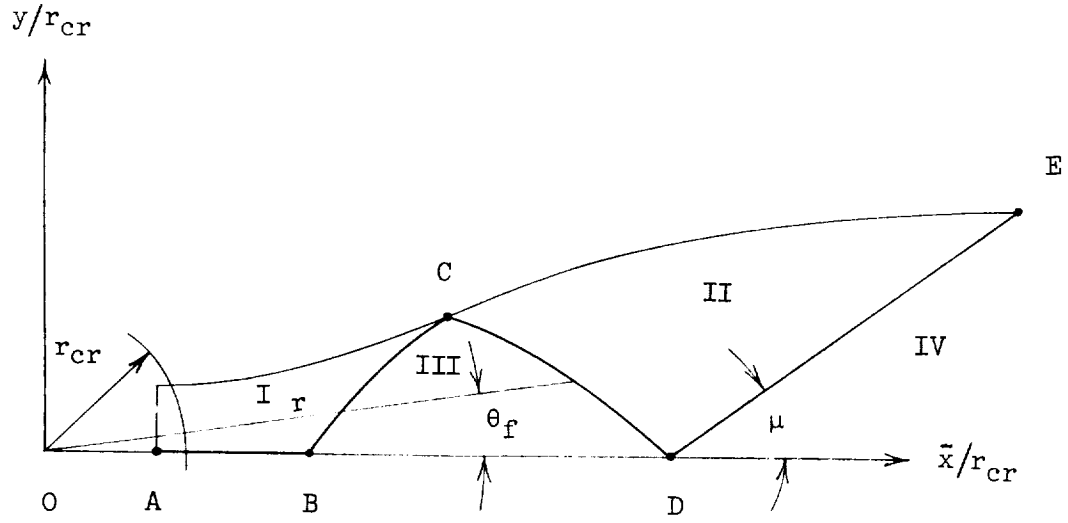


Sketch a

These quantities are based on real-gas considerations and are determined by a method presented in reference 13. For convenience in discussion, the nozzle is divided into four regions: I, first transition region; II, second transition region; III, radial flow; IV, uniform flow. Region III is bounded by the Mach lines BC and CD, and region IV is bounded by the final Mach line DE. The flow in region I is calculated by the method of characteristics and initial conditions along line ABC and the flow in region II is calculated by the method of characteristics and conditions along line CDE. The first task, then, is to calculate the flow conditions along line ABCDE.

Now the general equation for the radial-flow region as given by reference 13 is

$$\left(1 - M^2\right)\frac{du}{dr} + 2\,\frac{u}{r} = 0 \tag{A5}$$

For this region, the integrated characteristic equations, which are based on equation (A5), are

$$\theta_I = \int_0^{\theta_{f,I}} d\theta_f = \frac{1}{2} \int_{W(M=1)}^{W} \frac{\left(M^2 - 1\right)^{1/2}}{W}\, dW \tag{A6}$$

and

$$\int_{r_{cr}}^{r} \frac{dr}{r} = \frac{1}{2} \int_{W(M=1)}^{W} \frac{\left(M^2 - 1\right)}{W}\, dW \tag{A7}$$

Because M and, therefore, W are known at point D (sketch (a)), the value of $\theta_{I,D}$ at point D can be found by use of equation (A6) and the real-gas relation between M and W. Values of W, $\theta_f$, M, and $r/r_{cr}$ along line CD are determined by choosing values of W which are successively less than the value of W at point D. Values of $\theta_f$ for particular values of W are calculated from equation (A6) and from the real-gas relation between M and W, along with the condition that $\theta_f = \theta_{I,D} - \theta_I$ along the line CD. The corresponding values of $r/r_{cr}$ for these same values of W are determined from equation (A7) in a similar way. The coordinates for each of these calculations along line CD are determined from the equations

$$\frac{\bar{x}}{r_{cr}} = \frac{r}{r_{cr}} \cos \theta_f \tag{A8}$$

and

$$\frac{y}{r_{cr}} = \frac{r}{r_{cr}} \sin \theta_f \tag{A9}$$

The point indicated as C in sketch (a) is the nozzle-inflection point and corresponds to the maximum turning angle of the flow. The value of the flow angle at point C, $\theta_C$ is arbitrarily taken to be $12^o$ in this work. It follows then that the integrated angle at point C, $\theta_{I,C}$, as obtained from equation (A6), must equal the value determined from the condition that $\theta_C = \theta_{I,D} - \theta_{I,C}$. The values of M, W, $\bar{x}/r_{cr}$, and $y/r_{cr}$ at point C are fixed by equations (A7), (A8), and (A9).

The flow properties along line DE are all constant and equal to conditions at point D and are determined by the procedure just mentioned. It follows that the quantities W, $\theta_f$, $\bar{x}/r_{cr}$, $y/r_{cr}$, and M can be calculated along the boundary CDE and can serve as the starting conditions for calculation of flow in region II by the method of characteristics.

The flow properties along line BC are determined by the same method as they were along line CD, except that the flow angle along line BC is obtained from the condition that $\theta_f = \theta_I - \theta_{I,B}$, where $\theta_{I,B} = \theta_{I,D} - \theta_{I,C}$.

The required flow conditions along line AB are established by assuming a linear Mach number distribution with respect to $\bar{x}/r_{cr}$ from points A to B. This linear distribution is found by equating the slope of M with respect to $\bar{x}/r_{cr}$ as determined at point B to the slope in this linear portion. The value of $\bar{x}/r_{cr}$ for which the Mach number is unity is taken as the position of the throat of the nozzle. Inasmuch as the real-gas variation of W with respect to M has been determined, the establishment of a Mach number distribution along line AB also determines corresponding values of W along line AB. The necessary flow properties along line ABC can, therefore, be calculated so that the method of characteristics can be applied to determine the flow field in region I.

## Characteristic Mesh Size

The mesh size of the characteristic network is determined by the interval size between successive points chosen along the boundary line ABCDE. The intervals along lines BC and CD are determined by taking a constant interval of $r/r_{cr}$. The interval size along line DE was taken to be the same as along line CD. The intervals between points along AB can also be chosen arbitrarily. For a given Mach number and set of stagnation conditions, the inviscid contour was calculated for various mesh sizes in which the interval in $r/r_{cr}$ along line ABCDE was set equal to 0.1, 0.2, 0.25, and 0.3. The effect of mesh size on the calculated

contour based on these four values was found to be negligible. In addition, the inviscid contour was calculated along line AB for intervals of $r/r_{cr}$ of 0.05, 0.025, and 0.01 and for intervals along line BCDE of 0.1. The inviscid contour was again essentially unaffected by this change in mesh size. It may be concluded that these mesh sizes are small enough not to influence the inviscid result.

## Calculation of Characteristic Network for Real Gas

The characteristic network for a real gas is calculated by application of a method of successive approximations to equations (A1) and (A2), along with the tabulated real-gas values of $1/W^2$ and $1/M^2$ and the flow conditions along line ABCDE. This method is outlined in pages 264-265 of reference 12. It has been determined by trial and error that three successive approximations are sufficient to give satisfactory results at each point of calculation within the characteristic network.

## Calculation of Streamline Along Inviscid Boundary

Inasmuch as point C of sketch (a) is on the streamline which defines the inviscid boundary, the value of the stream function at any point along the inviscid boundary must be equal to the stream function at point C. The procedure for determining the streamline which corresponds to the inviscid boundary, then, first involves the calculation of the stream function at point C.

The differential form of the stream function in the radial-flow region as given in reference 13 is

$$d\psi = \rho u r^2 \sin \theta_f \, d\theta_f \tag{A10}$$

It is convenient to define a nondimensional stream function as

$$\bar{\psi} = \frac{\psi}{\rho_t u_l r_{cr}^2} \tag{A11}$$

Inasmuch as the flow properties are constant for a given value of $r/r_{cr}$ in the radial-flow region, the differential form of the stream function may be integrated for a particular value of $r/r_{cr}$ to yield

$$\bar{\psi} = \frac{\rho}{\rho_t} W \left(\frac{r}{r_{cr}}\right)^2 \left(1 - \cos \theta_f\right) \tag{A12}$$

The values of $W$, $r/r_{cr}$, and $\theta_f$ at point C can be found by a method already given. It is now required to know the real-gas relationship between $\rho/\rho_t$

and W. For the case of an ideal gas with a constant heat-capacity ratio, the relation between $\rho/\rho_t$ and W is

$$\frac{\rho}{\rho_t} = \left(1 - W^2\right)^{\frac{1}{\gamma-1}} \tag{A13}$$

The corresponding real-gas relation between $\rho/\rho_t$ and W is obtained from the form of equation (A13) and from tabulation of the quantity $\log \rho/\rho_t$ for various values of $\log\left(1 - W^2\right)$ as calculated for the real-gas isentropic expansion from a given stagnation condition. A plot of $\log \rho/\rho_t$ against $\log\left(1 - W^2\right)$ based on real-gas calculations showed that these quantities were nearly linear over small regions. Tabulated real-gas values of $\rho/\rho_t$ and W were used with linear interpolation between $\log \rho/\rho_t$ and $\log\left(1 - W^2\right)$ for intermediate values of $\rho/\rho_t$ and W for the calculation of $\bar{\psi}$ at point C by equation (A12). The value of the stream function $\bar{\psi}$ at any point on the inviscid contour must equal the stream function at point C, that is, $\bar{\psi} = \bar{\psi}_C$.

The general differential form of the stream function for axisymmetric flow as given in reference 13 is

$$d\psi = \rho y a \, ds \tag{A14}$$

where y is the distance from the axis, a is the local speed of sound, and ds is the differential distance along a Mach line. This equation can be integrated along a Mach line where s is taken as 0 at the axis, so that the nondimensional form of the stream function at any point s on a Mach line is

$$\bar{\psi} = \int_0^s \left(\frac{\rho}{\rho_t}\right) W (\sin \mu) \left(\frac{y}{r_{cr}^2}\right) ds \tag{A15}$$

The value of $\bar{\psi}$ is calculated at each point of the characteristic network by stepwise integration of equation (A15) in which the real-gas relation between $\rho/\rho_t$ and W is used. The location of the intersection of the inviscid boundary with any Mach line is determined when $\bar{\psi}$ for a particular Mach line is equal to $\bar{\psi}_C$. Points along the inviscid boundary are determined by interpolation between adjacent points in the network which have values of $\bar{\psi}$ that bound $\bar{\psi}_C$.

## Real-Gas Thermodynamic Properties

The calculations carried out in this work were based on the real-gas thermodynamic properties of nitrogen presented in references 7 and 8. These data were plotted and the various thermodynamic quantities along an isentropic expansion were determined and tabulated. These tabulated quantities M, W, and $\rho/\rho_t$ were then used directly in the machine calculations. The real-gas speed of sound for nitrogen above 100 atmospheres was based on the coefficients presented in reference 8.

## APPENDIX B

## BOUNDARY-LAYER CALCULATIONS

### General Procedure

After the inviscid contour has been determined from characteristic calculations, the boundary-layer displacement thickness along the nozzle must be added to obtain a physical-wall contour. The coordinate system for calculating the displacement thickness $\delta^*$ is shown in sketch (b).

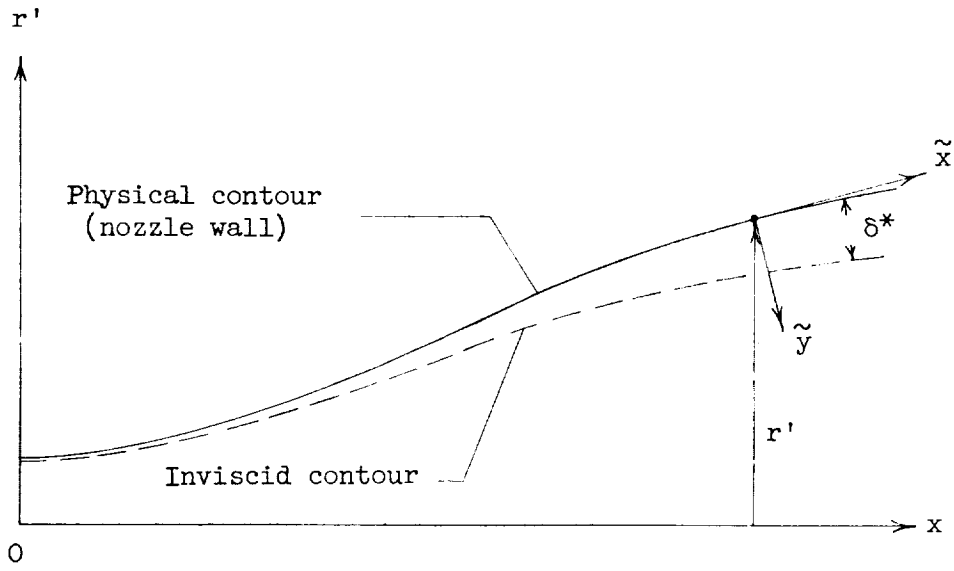


Sketch b

The flow quantities $u_1'$, $\rho_1$, and $M_1$ at the edge of the inviscid region, and the flow angle $\theta_f$ are known from the inviscid results. The corresponding values of the static temperature at the inviscid boundary $T_1$ was determined from tabulated real-gas values of $T_1$ against $M_1$ with linear interpolation between $1/T_1$ and $M_1^2$ for intermediate values.

The momentum equation used in this work as derived in reference 4 is

$$\frac{C_f}{2} = \frac{d\theta}{d\tilde{x}} + \left[\left(2 + \frac{\delta^*}{\theta}\right)\frac{1}{u_1'}\frac{du_1'}{d\tilde{x}} + \frac{1}{\rho_1}\frac{d\rho_1}{d\tilde{x}} + \frac{1}{r'}\frac{dr'}{d\tilde{x}}\right]\theta \qquad \text{(B1)}$$

where $r'$ is the radial distance to the nozzle wall. The derivatives of velocity, density, and radial distance with respect to distance along the nozzle wall $\tilde{x}$ are calculated from differences between flow properties at successive points along the inviscid boundary. The values of $\rho_1$ and $u_1$ were taken from the inviscid results at various locations.

## Calculation of Shape Parameter for Real Gas

The value of the shape parameter $\delta^*/\theta$ is calculated at each location with the following integral equations:

$$\frac{\delta^*}{\delta} = \int_0^1 \left(1 - \frac{\rho u'}{\rho_1 u_1'}\right) d\left(\frac{\tilde{y}}{\delta}\right) \tag{B2}$$

and

$$\frac{\theta}{\delta} = \int_0^1 \frac{\rho u'}{\rho_1 u_1'}\left(1 - \frac{u'}{u_1'}\right) d\left(\frac{\tilde{y}}{\delta}\right) \tag{B3}$$

The relation between the velocity profile and the variable of integration $\tilde{y}/\delta$ is assumed to be

$$\frac{u'}{u_1} = \left(\frac{\tilde{y}}{\delta}\right)^{1/N} \tag{B4}$$

The exponent $N$ in this relation is obtained at each location along the nozzle from the following correlation:

$$N = 1.77 \log N_{Re} - 0.38 - \frac{200}{N_{Re}} \tag{B5}$$

where $N_{Re}$ is based on local free-stream properties and the local value of the momentum thickness $\theta$. This correlation is similar to that presented in reference 14 and is based on experimental data for Mach numbers up to 9. This correlation was used to determine values of $N$ for values of $N_{Re}$ that are beyond the data for which this correlation was determined; however, the values of $\delta^*/\delta$ and $\theta/\delta$ have been found to be quite insensitive to $N$ at high values of $N$.

The evaluation of equations (B2) and (B3) also requires a relationship between the $u'/u_1'$ and $\rho/\rho_1$ within the boundary layer. This is obtained by beginning with the Crocco relation between total enthalpy and local velocity in the boundary layer as presented in reference 15.

$$H = A + B\left(\frac{u'}{u_1'}\right) \tag{B6}$$

where the total enthalpy at any point in the boundary layer is

$$H = h + \frac{(u')^2}{2} \tag{B7}$$

The constants A and B in equation (B6) are evaluated at the wall and at the edge of the boundary layer, so that the total enthalpy varies through the boundary layer according to the expression

$$H = h_w + \left(H_1 - h_w\right)\frac{u'}{u_1'} \tag{B8}$$

where $h_w$ is the static enthalpy at the wall.

The expression for the local static enthalpy, which includes real-gas effects due to vibration but no real-gas effects due to pressure, can be written in non-dimensional form as

$$\frac{h^o}{RT_b} = \left[\frac{7}{2}\frac{T}{T_b} + \frac{1}{T_b}\left(\frac{\Theta}{e^{\Theta/T} - 1}\right)\right] \tag{B9}$$

In order that the real-gas effects due to pressure on enthalpy be taken into account, equation (B9) is multiplied by a correction term which is equal to the actual real-gas enthalpy found in real-gas thermodynamic tables divided by the enthalpy calculated from equation (B9), both of which are taken at the same temperature. This correction term is denoted as $Q = h/h^o$, where $h^o$ represents the enthalpy at low pressures. It follows that Q is a function of temperature and pressure or any two thermodynamic functions. Since the entropy is constant in the inviscid flow region, the quantity Q along the inviscid boundary can be written as a function of pressure alone for a given stagnation condition. This quantity can be represented by a power series in $p_1$.

$$Q_1 = 1.0 + Ap_1 + B\left(p_1\right)^2 + C\left(p_1\right)^3 \tag{B10}$$

The wall temperature is known, therefore the correction term along the nozzle wall can also be expressed in a power series in pressure:

$$Q_w = 1.0 + Dp_1 + E\left(p_1\right)^2 + F\left(p_1\right)^3 \tag{B11}$$

where the coefficients A, B, C, D, E, and F in these equations are evaluated empirically from the real-gas thermodynamic data.

The variation of Q through the boundary layer was taken to be linear with respect to $h^o$ from the wall value $Q_w$ to the free-stream value $Q_1$. Plots

of Q against $h^{\circ}$ for various pressures were found to be approximately linear over a rather large range.

The equation which was used to relate the local velocity to the local density in the boundary layer was obtained by combining equations (B7), (B8), and (B9) and incorporating the pressure effect on enthalpy by the use of the function Q. The local temperature T within the boundary layer is replaced by the quantity $\frac{T_1}{\rho/\rho_1}$ so that the density and velocity within the boundary layer are related by the equation

$$Q\left[\frac{7}{2}\left(\frac{T_1/T_b}{\rho/\rho_1}\right) + \frac{\Theta/T_b}{e^{\frac{\Theta}{T_1}\left(\frac{\rho}{\rho_1}\right)} - 1}\right] = \frac{h_w}{RT_b}\left(1 - \frac{u'}{u_1'}\right) + \frac{H_1}{RT_b}\frac{u'}{u_1'} - \frac{1}{2}\frac{(u_1')^2}{RT_b}\left(\frac{u'}{u_1'}\right)^2 \qquad (B12)$$

The solution to the quantities $\delta^*/\delta$ and $\theta/\delta$ as defined by equations (B2) and (B3) is obtained by a quadrature method at any value of $\tilde{x}$ along the nozzle by simultaneous solution with equations (B4) and (B12).

## Skin-Friction Relation

The skin-friction relation presented in reference 5 was used in this work to calculate the local skin-friction coefficient. This skin-friction relation is represented by the following three equations:

$$\frac{C_f}{2} = (2ON)^{\frac{1-N}{1+N}}\left(\frac{\theta/\delta}{N_{Re}}\right)^{\frac{2}{N+1}}\left(\frac{T_1}{T_L}\right)^{\frac{N-2\omega-1}{N+1}} \qquad (B13)$$

$$\frac{T_L}{T_1} = \frac{T_w}{T_1} - \frac{T_w - T_{aw}}{T_1}\left(\frac{u_L}{u_1}\right) - \frac{T_{aw} - T_1}{T_1}\left(\frac{u_L}{u_1}\right)^2 \qquad (B14)$$

and

$$\frac{u_L}{u_1} = \left[\frac{2ON}{N_{Re}(\delta/\theta)}\right]^{\frac{1}{N+1}}\left(\frac{T_L}{T_1}\right)^{\frac{1+\omega}{N+1}} \qquad (B15)$$

Equations (B14) and (B15) are combined and solved by iteration at each point along the nozzle to determine $T_L$. The resulting value of $T_L$ is then used in equation (B13) to calculate $C_f/2$ at that position.

## Calculation of Momentum Thickness

The solution of equation (B1) requires an initial value of the momentum thickness $\theta$ at the point where $\tilde{x} = 0$. The effect of the magnitude of the assumed initial value of $\theta$ on the growth of $\theta$ along the nozzle was investigated by choice of initial values of $\theta$ of $10^{-2}$, $10^{-3}$, $10^{-4}$, and $10^{-5}$ inches. The results are shown in figure 17 which are based on the same inviscid conditions.

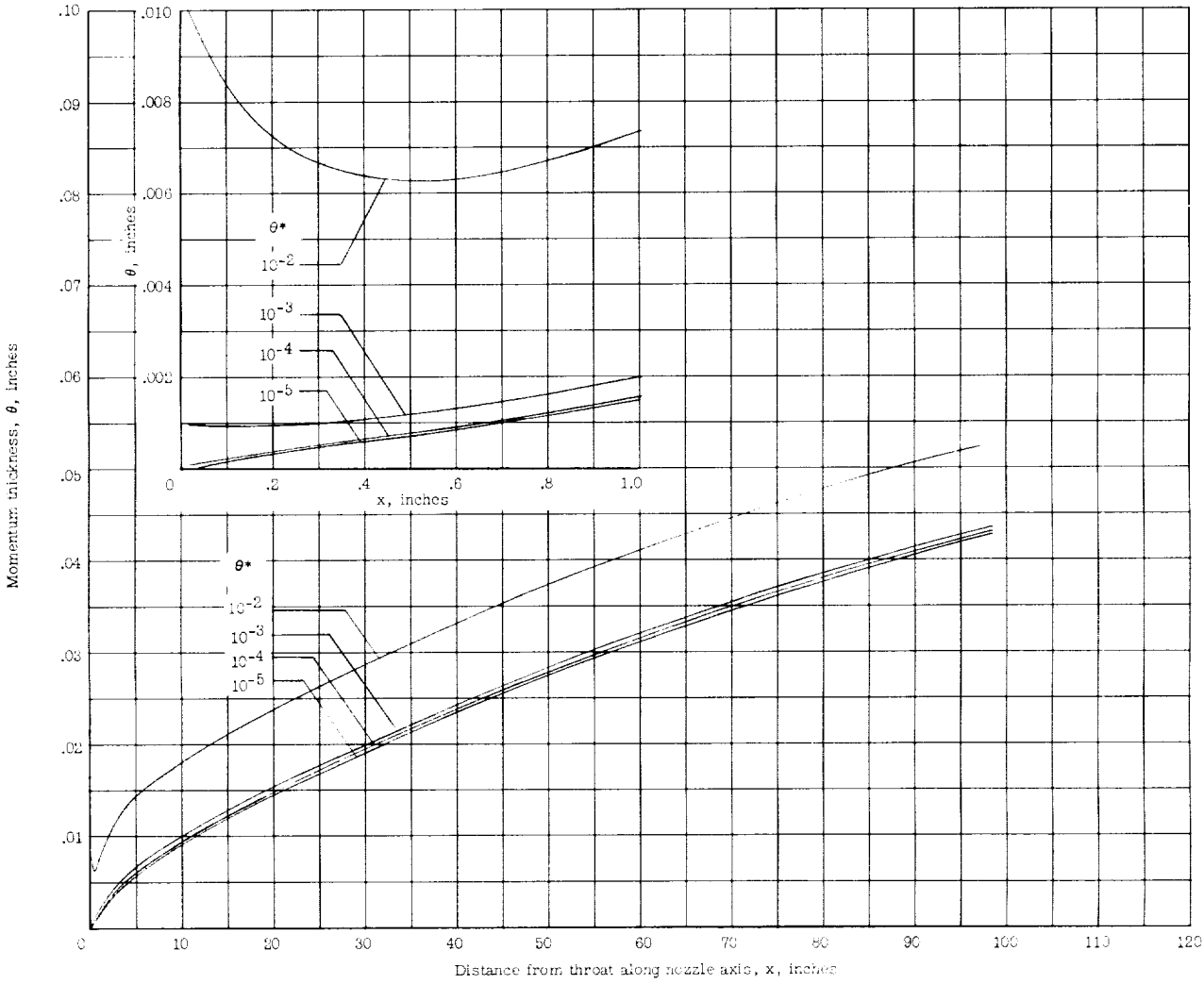


Figure 17.- Growth of real-gas boundary-layer momentum thickness as calculated for several values of throat momentum thickness $\theta^*$, at $M_1 = 17$, $p_t = 1{,}000$ atmospheres, $T_t = 4{,}200^\circ$ R, $T_w = 650^\circ$ R, and $d^* = 0.10$ inch.

It is seen that initial values of $\theta$ which are $10^{-4}$ or less do not significantly affect the values of $\theta$ downstream from the throat.

After the quantity $d\theta/d\tilde{x}$ is determined from equation (B1) at a particular location, values of $\theta$ for adjacent downstream locations are found in a stepwise manner.

## Nozzle Wall Temperature

The wall temperature enters into the calculation of $\delta^*$ in equations (B11), (B12), and (B14). Calculations for a constant wall temperature are straightforward. For a more realistic condition, the wall temperature was assumed to vary along the nozzle with the wall hot near the throat and cooler downstream. The expression used to describe these variations as a function of nozzle diameter ratio is

$$T_w = \frac{T_r - A(y/y^*)^{1.8}}{1 + B(y/y^*)^{1.8}} \tag{B16}$$

where $T_r$ is the gas temperature at the throat. The constants A and B are determined for an assumed wall temperature at the throat and an assumed wall temperature for a large value of $y/y^*$, respectively. This relation given by equation (B16) is based on a very rough heat balance between the nitrogen side of the nozzle and water-cooled passages in the nozzle wall. The term $(y/y^*)^{1.8}$ results from the assumption that the heat-transfer coefficient on the nitrogen side of the nozzle is proportional to the area ratio raised to 0.9 power, as indicated in reference 16. It should be noted that this expression for the variation of wall temperature along the nozzle was not developed to give an accurate prediction of wall temperature but, rather, to give a reasonable variation along the nozzle wall.

## Iterative Procedure for Determining Displacement Thickness

The first estimate of $\delta^*$ at a given nozzle position is found by assuming that the nozzle wall is represented by the inviscid contour. This initial value of $\delta^*$ is then added to the inviscid contour to give a better approximation of the physical wall. The value of $\delta^*$ based on this revised contour is then determined and compared with the previous value. The various gradients are also revised in the course of this procedure. This iteration process is repeated until successive calculations of $\delta^*$ at a given nozzle position differ by less than 0.001 inch.

## APPENDIX C

## COMPUTER PROGRAM FOR THE CALCULATION OF A NOZZLE CONTOUR

A computer program was developed for calculating hypersonic nozzle contours. This program is written in FORTRAN language (ref. 11) and is presented at the end of this appendix. This program facilitates the computation of the inviscid nozzle contour and the boundary-layer displacement thickness for a real gas based on the methods presented in appendixes A and B.

Part I of the program determines the flow properties along the boundaries of the inviscid flow region. A tabulation of $T$, $1/M^2$, $1/W^2$, $\rho/\rho_t$, based on a real gas, is supplied to the computer together with the flow angle at point C and the Mach number at point D (sketch (a)). The program prints the values of the flow properties of points A, B, C, and D. The program also writes on tape the flow properties along the boundaries DE, DC, BC, and BA. These properties are determined by the method described in appendix A.

Part II of the program computes the inviscid nozzle contour. The tabulation of $T$, $1/M^2$, $1/W^2$, and $\rho/\rho_t$ supplied in part I is also used in part II. The tape written by part I and containing the flow properties along the boundaries is used by part II. Beginning at point D the method of characteristics described in appendix A is used to determine the flow properties along upward-sloping characteristic lines in region II. These lines are computed from the boundary DC and are extended until the value of the stream function is equal to the stream function at point C. The final points on these characteristic lines define the inviscid nozzle contour from point E to point C. Continuing from point B, characteristic lines are computed in region I from the BA boundary and are extended until the value of the stream function is equal to the stream function at point C. The final points on these characteristic lines define the inviscid nozzle contour from point C to the throat. The flow properties of the points defining the inviscid nozzle contour are printed and also punched on cards for use in part III.

Part III computes the displacement thickness along the nozzle and applies it to the inviscid result to yield a physical contour. The flow properties at the edge of the inviscid region are supplied on cards punched by part II. The values of the constants used in equations (B10), (B11), (B16) and the variables such as $\rho_t$, $u_l$, $r_l$, $\omega$, $T_w$, and $T_r$ are supplied to the computer. The values of the shape parameter $\delta^*/\theta$, the skin-friction coefficient, and the momentum thickness $\theta$ are calculated at each point on the boundary as described in appendix B. An iterative procedure determines the value of the displacement thickness $\delta^*$. The value of $\delta^*$ is added to the inviscid contour to give a better approximation of the physical wall. Finally, a second-order interpolation is employed to locate points on the physical wall at desired increments. These interpolated points on the wall are then printed.

The following program has been used on the IBM 7090 electronic data processing system at the Langley Research Center to obtain the results presented herein.

```
     THESE ARE INPUTS REQUIRED FOR PART I  P-538.1
EMTAB=1/M2,INCREASING VALUES,LIMIT OF 100 VALUES
WTAB=1/W2,INCREASING VALUES LIMIT OF 100 VALUES
RHORT=RHO/RHOT,INCREASING VALUES LIMIT OF 100 VALUES
EMA=MACH NO. AT POINT A   TYPICALLY=1.
THETC=THETA AT POINT C IN RADIANS TYPICALLY=.2094395
EMD=MACH NO. AT POINT D  TYPICALLY=15.
N=NUMBER OF VALUES IN TABLE OF 1/M2
RLIM=LIMIT R/RCR ABOVE WHICH DELTA R/RCR IS KEPT
WITHIN RERR OF DRORCR TYPICALLY=4.90
RERR=ERROR LIMIT DR/RCR TYPICALLY=.02
DELW=DELTA W INTEGRATION INTERVAL  TYPICALLY=.001
DRORCR=DELTA R/RCR LIMIT
     ALSO DELTA R/RCR USED ON DE  TYPICALLY=.2
DDW=DELTA W REDUCTION  TYPICALLY=.000001
MAX=LIMIT TOTAL POINTS=2000
IBUG NOT=0 FOR EXTRA PRINT,=0 OMIT EXTRA PRINT
TTAB=T,DEGREES R,INCREASING VALUES,LIMIT OF 100 VALUES
DXBA=DELTA X ALONG BA  TYPICALLY=.025
DXDE=DELTA X ALONG DE  TYPICALLY=.2
     TOTAL NO. POINTS ON DE=(S/RCR+10)/DXDE



     THESE ARE INPUTS REQUIRED FOR PART II P-538.2
AREA=0 FOR CDE AREA,1. FOR ABC AREA,2. TO END CASE
START WITH CDE AREA
PRINT=0 TO PRINT WALL POINTS ONLY,=1. TO PRINT NET AND WALL POINTS
NAPRX=3=APPROXIMATIONS PER POINT
NN=NUMBER OF VALUES IN TABLE OF 1/M2



     THESE ARE INPUTS REQUIRED FOR PART III P-709.1
RHOT=RHO SUB T  TYPICALLY=6.300451
VE=V SUB L  TYPICALLY=8977.4414
R1=R SUB 1   TYPICALLY=55.159
C1=WHERE MU=(C1*T**3/2)/(T+D1+E1)   TYPICALLY=6.8873E-7
D1=CONSTANT IN MU EQUATION          TYPICALLY=1.
E1=CONSTANT IN MU EQUATION          TYPICALLY=180.
THI=THETA SUB I                     TYPICALLY=.0001
GC=32.1739
R=1774.688
THB=CHARACTERISTIC TEMPERATURE OF MOLECULAR VIBRATION TYPICALLY=6000.
OMEGA=EXPONENT IN VISCOSITY-TEMPERATURE RELATIONSHIP TYPICALLY=.76
TH=TW   TYPICALLY=650. R
ERR=ERROR TEST USE .00005
XM=SCALE FACTOR  TYPICALLY=.23832
TLTG=1.=TL/TI  TYPICALLY=1.
JLIM=TOTAL NO. OF POINTS ON WALL=NO. OF BINARY INPUT CARDS
DEBUG=0
N=32NO. OF POINTS PER INTERVAL GAUSS INTEGRATION
L=5NO. OF INTERVALS GAUSS INTEGRATION
ACASE=CASE NUMBER
ALPHA=WHERE Q=ALPHA+BETA*P+GAM*P**2+TAU*P**3 (EQ. B10) TYPICALLY=1.
BETA=CONSTANT IN Q EQUATION  TYPICALLY=.35463125E-7
GAM=CONSTANT IN Q EQUATION   TYPICALLY=-.153995146E-13
TAU=CONSTANT IN Q EQUATION   TYPICALLY=.42600556E-20
PR=P SUB R   TYPICALLY=.72
TTIG=T SUB T,1   TYPICALLY=5400.
T0=T SUB 0   TYPICALLY=491.688
AP=WHERE QW=AP+BP*P+CP*P**2+DP*P**3 (EQ. B10)  TYPICALLY=1.
BP=CONSTANT IN QW EQUATION                     TYPICALLY=.187295E-6
CP=CONSTANT IN QW EQUATION    TYPICALLY=.11277E-12
DP=CONSTANT IN QW EQUATION TYPICALLY=-.1472E-20
HT=IH SUB T,1I/(R*T SUB 0)  TYPICALLY=46.1817
APP=WHERE TW=(CPP-APP(Y/Y*)**1.8)/(1+BPP(Y/Y*)**1.8) (EQ. B16)
          TYPICALLY=0
BPP=CONSTANT IN TW EQUATION  TYPICALLY=0
CPP=CONSTANT IN TW EQUATION=TR       TYPICALLY=650.
YSTAR=CONSTANT IN TW EQUATION  TYPICALLY=1.
OPT=0 IF C=QI,NOT=0 IF Q NOT=QI
DIFN=ALLOWABLE DIFFERENCE IN N  TYPICALLY=.01
DIFD=ALLOWABLE DIFFERENCE IN DELTA STAR RELATIVE TO Y TYPICALLY=.0.1



P-538.1
PART I COMPUTES POINTS ALONG DE,DC,BC,BA AND
     SAVES THEM ON TAPE9
SUBROUTINE FINP IS FLOATING INPUT SUBROUTINE
SUBROUTINE BIRD READS BINARY CARDS
SUBROUTINE BIPUN PUNCHES BINARY CARDS
SUBROUTINE GAUSS PERFORMS INTEGRATION
SUBROUTINE RWCF FINDS SLOPE OF CURVE
DIMENSION WTAB(100),EMTAB(100),WLOGT(1001,RHOLNT(100),
```

```
     1RHORT(100),ALC(30),ALW(49),ALD(20),       W(2000),EM(2000),
     2RORCR(2000),THETI(2000),RORT(2000),AK(2000),THETBC(150),XBC(150),
     3XBA(1000),WBA(1000),YDC(150),WBC(150),THETDC(800),XDC(800),
     4YDC(800),PSIDC(800),WDC(800),RORTDC(800),YDE(3400),XDE(3400)
     5,TTAB(100),EMSQT(100),TEMP(100)
      DIMENSION DER(110)
      EQUIVALENCE (EMTAB,DUMMY1),(WTAB,DUMMY2),(WLOGT,DUMMY3),(RHOLNT,
     1DUMMY4),(TTAB,DUMMY5),(EMSQT,DUMMY6)
      EQUIVALENCE(W,XDE),(EM,XDE(2001)),(EM(1401),YDE),
     1(RORCR,YDE(601)),(THETI,YDE(2601)),(THETI(801),XBA),
     2(THETI(1801),WBA),(RORT,WBA(201))
      COMMON EMTAB,WTAB,WLOGT,RHOLNT,TTAB,EMSQT
      COMMON RHORT,EMA,THETC,EMD,N,DSDE,DMBA,DW,DRORCR,
     1DDW,MAX
C     READS INPUT CARDS
C     FINP IS FLOATING INPUT SUBROUTINE
      CALLFINP(17,EMTAB,WTAB,RHORT,EMA,THETC,EMD,N,RLIM,
     1RERR,DELW,DRORCR,DDW,MAX,IBUG,TTAB,DXBA,DXDE)
C     WRITES HEAD
      WRITE OUTPUT TAPE 6,305
C     COMPUTES 1/T,M2,W,LOGE(1-W2),LOGE(RHO/RHOT)
      DO 4 I=1,N
      TTAB(I)=1./TTAB(I)
      EMSQT(I)=1./EMTAB(I)
      WN=SQRTF(1./WTAB(I))
      WLOGT(I)=LOGF(1.-WN**2)
    4 RHOLNT(I)=LOGF(RHORT(I))
C     REVERSES 1/T TABLE
      K=N
      DO 1000 I=1,N
      TEMP(K)=TTAB(I)
 1000 K=K-1
      DO 2000 I=1,N
 2000 TTAB(I)=TEMP(I)
C     REVERSES M2 TABLE
      K=N
      DO 3000 I=1,N
      TEMP(K)=EMSQT(I)
 3000 K=K-1
      DO 4000 I=1,N
 4000 EMSQT(I)=TEMP(I)
C     COMPUTES 1/MA2 AND INTERPOLATES 1/WA2
      OVMA=1./EMA**2
C     FTLUP IS FLOATING TABLE LOOK UP AND INTERPOLATION SUBROUTINE
      CALL FTLUP(OVMA,OVWA,1,N,EMTAB,WTAB)
C     COMPUTES 1/MD2 AND INTERPOLATES 1/WD2
      OVMD=1./EMD**2
      CALL FTLUP(OVMD,OVWD,1,N,EMTAB,WTAB)
C     COMPUTES WA
      WA=SQRTF(1./OVWA)
C     COMPUTES WD
      WD=SQRTF(1./OVWD)
C     SET R/RCR=1
      RORCR(1)=1.
C     SET SUM=0
      SUM=0
C     SET SUM2=0
      SUM2=0
C     INTEGRATION BY TRAPEZOIDAL RULE FROM WA TO WD OF (M2-1)/W AND SQT
C          (M2-1)/W
      ZTERM=(EMA**2-1.)/WA
      ZTERM2=(SQRTF(EMA**2-1.))/WA
      DW=DELW
C     COMPUTE WA POINT
      W(1)=WA
      ICOUNT=0
C     TURN OFF LIGHT
      IF(SENSE LIGHT 1)8,8
C     COMPUTES W,M,R/RCR,THETAI,RHO/RHOT,K,LIMIT OF2000 POINTS
    8 DO 12 I=2,MAX
    9 W(I)=W(I-1)+DW
      IF(W(I)-WD)7,7,113
  113 IF(SENSE LIGHT 1) 115,116
  116 DW=WD-W(I-1)
      SENSE LIGHT 1
      GO TO 9
    7 OVW=1./W(I)**2
      CALL FTLUP(OVW,OVM,1,N,WTAB,EMTAB)
      EM(I)=SQRTF(1./OVM)
      TEMP=(EM(I)*EM(I)-1.)
      TEMP1=TEMP/W(I)
      TEMP2=SQRTF(TEMP)/W(I)
      TEMP4=(ZTERM+TEMP1)*.5*DW+SUM
C     EQUATION A7
      RORCR(I)=EXPF(.5*TEMP4)
      IF(SENSE LIGHT 2)611,609
  611 SENSE LIGHT 2
  608 IF(SENSE LIGHT 3)610,609
  610 RERR=RLRR+.01
      IF(SENSE LIGHT 2)609,609
  609 IF(RORCR(I)-RLIM)10,602,602
  602 IF(ABSF(RORCR(I)-RORCR(I-1)-DRORCR)-RERR)10,10,603
  603 IF(RORCR(I)-RORCR(I-1)-DRORCR)604.10
  605 DW=DW-DDW
      SENSE LIGHT 2
      IF(IBUG)5000,5001,5000
 5000 WRITEOUTPUTAPE6,302,W(I),DW,RORCR(I)
 5001 GOTO9
  604 DW=DW+DDW
      SENSE LIGHT 3
      IF(IBUG)5002,5003,5002
 5002 WRITEOUTPUTAPE6,302,W(I),DW,RORCR(I)
```

```
 5003 GOTO9
   10 TEMP3=(ZTERM2+TEMP2)*.5*DW+SUM2
      IF(SENSE LIGHT 2)606,606
  606 IF(SENSE LIGHT 3)607,607
  607 IF(IBUG)5004,5005,5004
 5004 WRITE OUTPUT TAPE6,302,W(I),DW,RORCR(I)
C     EQUATION A6
 5005 THETI(I)=.5*TEMP3
      ZTERM=TEMP1
      ZTERM2=TEMP2
      SUM=TEMP4
      SUM2=TEMP3
      WLOG=LOGF(1.-W(I)**2)
      CALL FTLUP(WLOG,RHOLN,1,N,WLOGT,RHOLNT)
      RORT(I)=EXPF(RHOLN)
      ICOUNT=ICOUNT+1
      IF(ICOUNT-2000)12,12,1600
   12 AK(I)=(OVW-1.)/OVM
C     ICOUNT=NO OF THETAS AND RORCRS STARTING WITH THETI(2)AND RORCR(2)
C     COMPUTE THETAID AND THETAIC
  115 THETID=THETI(ICOUNT+1)
C     COMPUTE THETAI,W,R/RCR,M,K AT POINT B
      THETIB=THETID-2.*THETC
      THETIC=THETID-THETC
      CALL FTLUP(THETIB,WB,1,ICOUNT,THETI(2),W(2))
      CALL FTLUP(THETIB,RORCRB,1,ICOUNT,THETI(2),RORCR(2))
      OVWB=1./WB**2
      CALL FTLUP(OVWB,OVMB,1,N,WTAB,EMTAB)
      EMB=SQRTF(1./OVMB)
      AKB=(OVWB-1.)/OVMB
C     FIT CURVE TO 7 POINTS AND READ DK/DMB AT POINT B
C     STORE KS IN ALD BLOCK
      J=2
      DO 100 I=2,ICOUNT
      IF(EM(I+3)-EMB) 100,100,102
  102 ALD(J)=EM(I)
      ALD(J-1)=AK(I)
      J=J+2
      IF(J-8) 101,103,101
  103 J=J+2
  101 IF(J-16) 100,104,104
  100 CONTINUE
  104 ALD(8)=EMB
      ALD(7)=AKB
C     SHARE SUBROUTINE RWCF IS USED FOR SECOND DEGREE POLYNOMIAL
C     LEAST SQUARES CURVE FITTING ROUTINE USING ORTHOGONAL POLYNOMONIALS
      CALL CF2F1(3,ALC,0,ALW,ALD,2,7)
      CALL CF2F2(EMB,ALC,2,DER,1,2)
      DKDMB=DER(3)
C     COMPUTE W,R/RCR,M,RHO/RHOT,K,XBAR,Y,PSI AT POINT C
      CALL FTLUP(THETIC,WC,1,ICOUNT,THETI(2),W(2))
      CALL FTLUP(THETIC,RORCRC,1,ICOUNT,THETI(2),RORCR(2))
      OVWC=1./WC**2
      CALL FTLUP(OVWC,OVMC,1,N,WTAB,EMTAB)
      EMC=SQRTF(1./OVMC)
      WLOGC=LOGF(1.-WC**2)
      CALL FTLUP(WLOGC,RHOLNC,1,N,WLOGT,RHOLNT)
      RORTC=EXPF(RHOLNC)
      AKC=(OVWC-1.)/OVMC
C     EQUATION A9
      YC=RORCRC*SINF(THETC)
C     EQUATION A12
      PSIC=RORTC*WC*RORCRC**2*(1.-COSF(THETC))
C     COMPUTE DM/DRORCR AT POINT B
      DMDR=2./((WB/EMB)**2*(1.-EMB**2)*RORCRB*(1.5*
     1DKDMB-AKB/EMB))
C     COMPUTE R/RCR AT POINT A
      RORCRA=RORCRB-(EMB-EMA)/DMDR
C     COMPUTE X AT POINT C
      XC=RORCRC*COSF(THETC)-RORCRA
      NABPTS=0
      NBCPTS=0
      NDCPTS=0
      K=1
      J=1
 4001 L=ICOUNT+1
      DO 300 I=2,L
 4002 IF(THETI(I)-THETIB) 17,16,16
   16 IF(THETI(I)-THETIC) 13,14,14
C     COMPUTE THETA,Y,W,X AT POINTS ALONG BC LIMIT OF 150 POINTS
   13 THETBC(J)=THETI(I)-THETIB
C     EQUATION A9
      YBC(J)=RORCR(I)*SINF(THETBC(J))
      WBC(J)=W(I)
      XBC(J)=RORCR(I)*COSF(THETBC(J))-RORCRA
      NBCPTS=NBCPTS+1
      IF(J-150)1300,1300,1600
C     IF NO. OF POINTS EXCEEDS STORAGE,PRINT OUT HERE
C           AND STOP
 1600 WRITE OUTPUT TAPE 6,500,J,K,I,ICOUNT
      CALL EXIT
 1300 J=J+1
      GO TO 300
C     COMPUTE THETA,X,Y,PSI,W,RHO/RHOT AT POINTS ALONG CD LIMIT OF 800
C          POINTS
   14 THETDC(K)=THETID-THETI(I)
      XDC(K)=RORCR(I)*COSF(THETDC(K))-RORCRA
C     EQUATION A9
      YDC(K)=RORCR(I)*SINF(THETDC(K))
C     EQUATION A12
      PSIDC(K)=RORT(I)*W(I)*RORCR(I)**2*(1.-COSF(THETDC(K)))
      WDC(K)=W(I)
```

```
      NDCPTS=NDCPTS+1
      RORTDC(K)=RORT(I)
      IF(K-300)1400,1400,1600
 1400 K=K+1
      GO TO 300
   17 NABPTS=NABPTS+1
  300 CONTINUE
  400 NAB=0
      DX=0
      XB=RORCRB-RORCRA
      SAVE=RORT(ICOUNT+1)
      SAVE2=RORCR(ICOUNT+1)
C     COMPUTE POINTS ALONG BA LIMIT OF 1000
      DO22I=1,MAX
      XBA(I)=XB-DX
      IF(XBA(I))600,601,601
  600 XBA(I)=0
  601 TEM =XBA(I)*DMDR+1.
      OVM=1./(TEM )**2
      CALL FTLUP(OVM,OVW,1,N,EMTAB,WTAB)
      WBA(I)=SQRTF(1./OVW)
      IF(I-1000)1500,1500,1600
 1500 NAB=NAB+1
      IF(XBA(I))22,23,22
   22 DX=DX+DXBA
C     COMPUTE S/RCR AT POINT D
   23 SORCR=SQRTF((2.*PSIC)/(SAVE           *(WD/EMD**2)))
C     ENDE=NUMBER OF POINTS ON DE LIMIT OF 3400
      ENDE=(SORCR+10.)/DXDE
      EMUD=ARTNCF(1./EMD,SQRTF(1./EMD)**2)
      NDE=ENDE
      DSSMU=DRORCR*SINF(EMUD)
      DSCMU=DRORCR*COSF(EMUD)
      FLT=1.
      DO 211 I=1,NDE
C     COMPUTE X,Y OF POINTS ALONG DE
      XDE(I)=XDC(NDCPTS)+FLT*DSCMU
      YDE(I)=FLT*DSSMU
      IF(I-3400)211,211,1600
  211 FLT=FLT+1.
      RORCRD=SAVE2
C     WRITES DM/DRORCR AT POINT B
      WRITE OUTPUT TAPE 6,301,DMDR
      XA=0
      YA=0
      THETAA=0
      XB=RORCRB-RORCRA
      YB=0
      YD=0
C     WRITES HEADING
C     WRITES THETA,X,Y,W,M,R/RCR FOR A,B,C,D POINTS
      WRITE OUTPUT TAPE 6,303
      WRITE OUTPUT TAPE 6,310,XA,YA,EMA,WA,RORCRA,THETAA
      WRITE OUTPUT TAPE 6,303
      WRITE OUTPUT TAPE 6,311,XB,YB,EMB,WB,RORCRB,THETB
      WRITE OUTPUT TAPE 6,303
      WRITE OUTPUT TAPE 6,312,XC,YC,EMC,WC,RORCRC,THETC
      WRITE OUTPUT TAPE 6,303
      WRITE OUTPUT TAPE 6,313,XDC(NDCPTS),YD,EMD,WD,RORCRD,THETD
  303 FORMAT(1H 10X1HX16X1HY16X1HM16X1HW14X5HR/RCR8X6HTHETAI)
  310 FORMAT(3H A=1E16.8,5E16.8)
  311 FORMAT(3H B=1E16.8,5E16.8)
  312 FORMAT(3H C=1E16.8,5E16.8)
  313 FORMAT(3H D=1E16.8,5E16.8)
  306 N=4*NDE
C     WRITE TAPE 9 SAVING INFORMATION ABOUT ALL POINTS ON AB,BC,CD,DE
      REWIND 9
      WRITE TAPE 9,PSIC,WD,N,(XDE(L),YDE(L),L=1,NDE)
      K=NDCPTS
      DO 405 I=1,NDCPTS
  404 WRITE TAPE 9,(XDC(K),YDC(K),THETDC(K),WDC(K),PSIDC(K),
     1RORTDC(K))
  405 K=K-1
      ZERO=0
      WRITE TAPE 9,(ZERO,ZERO,ZERO,ZERO,ZERO,ZERO)
      N=4*(NBCPTS+1)
      WRITE TAPE 9,PSIC,N,(XBC(I),YBC(I),THETBC(I),WBC(I),I=1,NBCPTS)
      WRITE TAPE 9,XC,YC,THETC,WC
      DO 403 I=1,NAB
  403 WRITE TAPE 9, XBA(I),WBA(I)
      WRITE TAPE 9, ZERO,ZERO
      REWIND 9
C     TABLES ARE SAVED IN COMMON STORAGE FOR NEXT CHAIN
      CALL CHAIN (2,83)
  302 FORMAT(6E19.8)
  304 FORMAT(4E19.8)
  301 FORMAT(6H DMDR=1E19.8)
  305 FORMAT(9H1P-538.1/)
  500 FORMAT(4I12)
      END




C     P-538.2
C     PART II  NOZZLE CALCULATION
C     TABLES ARE ALREADY IN COMMON STORAGE FROM PREVIOUS CHAIN
C     PART II COMPUTES POINTS ALONG WALL FROM E TO C
C          AND FROM C TO THROAT,
C          PSI ALONG WALL=PSI AT POINT C
```

```
C          PUNCHES X,Y,M,W,RHO/RHOT,THETA,T OF WALL POINTS
      DIMENSION STOR(4000),TEMP(101,EMTAB(100),WTAB(100),WLOGT(100),
     1RHOLNT(100)
     2,TTAB(100),EMSQT(100)
      EQUIVALENCE (EMTAB,DUMMY1),(WTAB,DUMMY2),(WLOGT,DUMMY3),(RHOLNT,
     1DUMMY4),(TTAB,DUMMY5),(EMSQT,DUMMY6)
      COMMON EMTAB,WTAB,WLOGT,RHOLNT,TTAB,EMSQT
      COMMON XA,YA,THA,WA,FA,PSIA,XB,YB,THB,WB,XC,YC,THC,WC,FC,PSIC,AMC,
     1AMUC,SMUC,CMUC,TMUC,PPC,YAV,THAV,WAV,AMAV,AMUAV,SMUAV,CMUAV,TMUAV,
     2STHAV,YBV,THBV,WBV,AMBV,AMUBV,SMUBV,CMUBV,TMUBV,STHCV,XLIM,YLIM,
     3AMLIM,WLIM,PPLIM,THLIM,TLIM,PLIM,AMUL,SMLIM,CMLIM,TMLIM,THPM,
     4TANP,THPM,SINM,COSM,TANM,XATY,ACL,BCM,TEMP,WD,P,N,I,J,AREA,PRINT,
     5NAPRX,NN,ALNW,ALNP
     6,SINP,COSP,STOR
      FLIMF(XC,XA,P)=P*(XC-XA)+XA
      REWIND 9
C     TAPE 9 FROM CHAIN 1 CONTAINS
C     REC 1 PSIC,WD,4NDE,X AND Y OF ALL PTS D+1 TO E
C     REC 2 X,Y,THETA,W,PSI,RHO/RHOT OF EACH PT D TOC-1
C     -------
C     REC(2+NDCPTS) 0,0,0,0,0,0
C     REC(3+NDCPTS) PSIC,4(NBCPTS+1),X,Y,THETA,W OF ALL PTS B+1 TO C-1
C     REC(4+NDCPTS) X,Y,THETA,W OF PT C
C     REC(5+NDCPTS) X,W OF EACH PT B TO A+1
C     -------
C     REC(5+NDCPTS+NABPTS) 0,C
   28 CALL FINP(4,AREA,PRINT,NAPRX,NN)
      IF(AREA-1.) 41,41,40
   40 CALL CHAIN(1,B3I
C     READ IN A LINE TO STOR
C     READ IN PT ON B LINE TO C PT
   41 WRITE OUTPUT TAPE 6,132
      IF(AREA) 18,19,18
   18 READ TAPE 9,PLIM,N,(STOR(J),J=5,N)
      K=N+4
      I=N+1
      READ TAPE 9,(STOR(J),J=I,K)
      XLIM=STOR(N+1)
      YLIM=STOR(N+2)
      CALL AMCMU(STOR(N+4),SMLIM,TMLIM,AMUL,AMLIM,CMLIM)
      THLIM=STOR(N+3)
      WLIM=STOR(N+4)
      CALL PPT(WLIM,PPLIM)
      EMSQ=AMLIM*AMLIM
C     SUBROUTINE FTLUP INTERPOLATES IN TABLE
      CALL FTLUP(EMSQ,TLIM,1,NN,EMSQT(1),TTAB(1))
      TLIM=1./TLIM
      CALL BIPUN(XLIM,TLIM)
      WRITE OUTPUT TAPE6,100,XLIM,YLIM,AMLIM,WLIM,PPLIM,THLIM,TLIM
      READ TAPE 9,(STOR(1),STOR(4))
      STOR(2)=0.
      STOR(3)=0.
      GO TO 22
C     READ IN LINE DE AND A POINT FROM DC
   19 READ TAPE 9,PLIM,WD,N,(STOR(J),STOR(J+1),J=1,N,4)
      READ TAPE 9,XC,YC,THC,WC,PSIC,PPC
      DO 21 J=1,N,4
C     THETA=0 AND W=WD FOR ALL PTS ON DE
      STOR(J+2)=0.
   21 STOR(J+3)=WD
   20 IF(AREA) 22,23,22
   22 READ TAPE 9,XC,WC
C     Y=0,THETA=0,F=0,PSI=0 FOR ALL PTS ON BA
      YC=0.
      THC=0.
      FC=0.
      PSIC=0.
      GO TO 24
C     READ IN NEXT POINT FROM DC AND COMPUTE NEXT LINE
   23 READ TAPE 9,XC,YC,THC,WC,PSIC,PPC
      CALL AMCMU(WC,SMUC,TMUC,AMUC,AMC,CMUC)
      FC=PPC*WC*YC*SMUC
   24 IF(WC) 25,28,25
C     AFTER C IS COMPUTED MOVE STOR TO B AND MOVE C TO A AND TO STOR
C     WHEN PSI REACHES LIMIT COMPUTE END PT
   25 IF(AREA) 10,11,10
   10 N=1
      GO TO 7
   11 N=5
      GO TO 7
    6 N=N+4
    7 XB=STOR(N)
      YB=STOR(N+1)
      THB=STOR(N+2)
      WB=STOR(N+3)
      XA=XC
      YA=YC
      THA=THC
      WA=WC
      FA=FC
      PSIA=PSIC
      IF(AREA) 12,13,12
   12 STOR(N)=XC
      STOR(N+1)=YC
      STOR(N+2)=THC
      STOR(N+3)=WC
      GO TO 14
   13 STOR(N-4)=XC
      STOR(N-3)=YC
      STOR(N-2)=THC
      STOR(N-1)=WC
   14 CALL GENPT
```

```
      IF(PRINT) 27,26,27
   27 WRITE OUTPUT TAPE 6,100,XA,YA,THA,WA,FA,PSIA,XB,YB,THB,WB,XC,YC,
     1AMC,WC,PSIC,PPC,FC,THC,AMUC
C     COMPUTE ALONG AN UPWARD SLOPING CHARACTERISTIC LINE UNTIL PSI
C        LIMIT IS REACHED
   26 IF(PSIC-PLIM) 6,8,8
    8 IF(AREA) 15,16,15
   15 STOR(N+4)=XC
      STOR(N+5)=YC
      STOR(N+6)=THC
      STOR(N+7)=WC
      GO TO 17
   16 STOR(N)=XC
      STOR(N+1)=YC
      STOR(N+2)=THC
      STOR(N+3)=WC
   17 P=(PLIM-PSIA)/(PSIC-PSIA)
      XLIM=FLIMF(XC,XA,P)
      YLIM=FLIMF(YC,YA,P)
      THLIM=FLIMF(THC,THA,P)
      WLIM=FLIMF(WC,WA,P)
      CALL AMCMU(WLIM,SMLIM,TMLIM,AMUL,AMLIM,CMLIM)
      CALL PPT(WLIM,PPLIM)
      EMSQ=AMLIM*AMLIM
      CALL FTLUP(EMSQ,TLIM,1,NN,EMSQT(1),TTAB(1))
      TLIM=1./TLIM
C     PUNCH X,Y,M,W,RHO/RHOT,THETA,T
      CALL BIPUN(XLIM,TLIM)
  101 FORMAT(1H 3E16.8)
C     PRINTS X,Y,M,W,RHO/RHOT,THETA,T OF WALL POINTS
      WRITE OUTPUT TAPE6,100,XLIM,YLIM,AMLIM,WLIM,PPLIM,THLIM,TLIM
  100 FORMAT(1H 7E16.8)
  102 FORMAT(1H 7X1HX16X1HY16X1HM16X1HW11X8HRHO/RHOT9X5HTHETA13X1HT)
      GO TO 23
      END



      SUBROUTINE PSI(WX,PPX)
C     SUBROUTINE PSI COMPUTES PSI GIVEN W AND RHO/RHOT
      DIMENSION STOR(4000),TEMP(10),EMTAB(100),WTAB(100),WLOGT(100),
     1RHOLNT(100)
     2,TTAB(100),EMSQT(100)
      EQUIVALENCE (EMTAB,DUMMY1),(WTAB,DUMMY2),(WLOGT,DUMMY3),(RHOLNT,
     1DUMMY4),(TTAB,DUMMY5),(EMSQT,DUMMY6)
      COMMON EMTAB,WTAB,WLOGT,RHOLNT,TTAB,EMSQT
      COMMON XA,YA,THA,WA,FA,PSIA,XB,YB,THB,WB,XC,YC,THC,WC,FC,PSIC,AMC,
     1AMUC,SMUC,CMUC,TMUC,PPC,YAV,THAV,WAV,AMAV,AMUAV,SMUAV,CMUAV,TMUAV,
     2STHAV,YBV,THBV,WBV,AMBV,AMUBV,SMUBV,CMUBV,TMUBV,STHBV,XLIM,YLIM,
     3AMLIM,WLIM,PPLIM,THLIM,TLIM,PLIM,AMUL,SMLIM,CMLIM,TMLIM,THPM,
     4TANP,THMM,SINM,COSM,TANM,XATY,ACL,BCM,TEMP,WD,P,N,I,J,AREA,PRINT,
     5NAPRX,NN,ALNW,ALNP,STOR
     6,SINP,COSP
      CALL PPT(WX,PPX)
      FC=PPX*WX*YC*SMUC
      PSIC=PSIA+.5*(FA+FC)*SQRTF((XC-XA)*(XC-XA)+(YC-YA)*(YC-YA))
      RETURN
      END



      SUBROUTINE PPT(WX,PPX)
C     SUBROUTINE PPT COMPUTES RHO/RHOT GIVEN W
      DIMENSION STOR(4000),TEMP(10),EMTAB(100),WTAB(100),WLOGT(100),
     1RHOLNT(100)
     2,TTAB(100),EMSQT(100)
      EQUIVALENCE (EMTAB,DUMMY1),(WTAB,DUMMY2),(WLOGT,DUMMY3),(RHOLNT,
     1DUMMY4),(TTAB,DUMMY5),(EMSQT,DUMMY6)
      COMMON EMTAB,WTAB,WLOGT,RHOLNT,TTAB,EMSQT
      COMMON XA,YA,THA,WA,FA,PSIA,XB,YB,THB,WB,XC,YC,THC,WC,FC,PSIC,AMC,
     1AMUC,SMUC,CMUC,TMUC,PPC,YAV,THAV,WAV,AMAV,AMUAV,SMUAV,CMUAV,TMUAV,
     2STHAV,YBV,THBV,WBV,AMBV,AMUBV,SMUBV,CMUBV,TMUBV,STHBV,XLIM,YLIM,
     3AMLIM,WLIM,PPLIM,THLIM,TLIM,PLIM,AMUL,SMLIM,CMLIM,TMLIM,THPM,
     4TANP,THMM,SINM,COSM,TANM,XATY,ACL,BCM,TEMP,WD,P,N,I,J,AREA,PRINT,
     5NAPRX,NN,ALNW,ALNP,STOR
     6,SINP,COSP
      ALNW=LOGF(1.-WX*WX)
      CALL FTLUP(ALNW,ALNP,1,NN,WLOGT(1),RHOLNT(1))
      PPX=EXPF(ALNP)
      RETURN
      END



      SUBROUTINE THM(THX,TANX,COSX,AMUX,THMX,SINX)
C     SUBROUTINE THM COMPUTES COS,SIN,TAN OF (THETA-MU) GIVEN THETA AND
C        MU
      DIMENSION STOR(4000),TEMP(10),EMTAB(100),WTAB(100),WLOGT(100),
     1RHOLNT(100)
     2,TTAB(100),EMSQT(100)
      EQUIVALENCE (EMTAB,DUMMY1),(WTAB,DUMMY2),(WLOGT,DUMMY3),(RHOLNT,
     1DUMMY4),(TTAB,DUMMY5),(EMSQT,DUMMY6)
      COMMON EMTAB,WTAB,WLOGT,RHOLNT,TTAB,EMSQT
      COMMON XA,YA,THA,WA,FA,PSIA,XB,YB,THB,WB,XC,YC,THC,WC,FC,PSIC,AMC,
     1AMUC,SMUC,CMUC,TMUC,PPC,YAV,THAV,WAV,AMAV,AMUAV,SMUAV,CMUAV,TMUAV,
     2STHAV,YBV,THBV,WBV,AMBV,AMUBV,SMUBV,CMUBV,TMUBV,STHBV,XLIM,YLIM,
     3AMLIM,WLIM,PPLIM,THLIM,TLIM,PLIM,AMUL,SMLIM,CMLIM,TMLIM,THPM,
     4TANP,THMM,SINM,COSM,TANM,XATY,ACL,BCM,TEMP,WD,P,N,I,J,AREA,PRINT,
     5NAPRX,NN,ALNW,ALNP,STOR
     6,SINP,COSP
      THMX=THX-AMUX
      COSX=COSF(THMX)
```

```
      SINX=SINF(THMX)
      TANX=SINX/COSX
      RETURN
      END


      SUBROUTINE THP(THX,TANX,COSX,AMUX,THPX,SINX)
C     SUBROUTINE THP COMPUTES COS,SIN,TAN OF (THETA+MU) GIVEN THETA AND
C         MU
      DIMENSION STOR(4000),TEMP(10),EMTAB(100),WTAB(100),WLOGT(100),
     1RHOLNT(100)
     2,TTAB(100),EMSQT(100)
      EQUIVALENCE (EMTAB,DUMMY1),(WTAB,DUMMY2),(WLOGT,DUMMY3),(RHOLNT,
     1DUMMY4),(TTAB,DUMMY5),(EMSQT,DUMMY6)
      COMMON EMTAB,WTAB,WLOGT,RHOLNT,TTAB,EMSQT
      COMMON XA,YA,THA,WA,FA,PSIA,XB,YB,THB,WB,XC,YC,THC,WC,FC,PSIC,AMC,
     1AMUC,SMUC,CMUC,TMUC,PPC,YAV,THAV,WAV,AMAV,AMUAV,SMUAV,CMUAV,TMUAV,
     2STHAV,YBV,THBV,WBV,AMBV,AMUBV,SMUBV,CMUBV,TMUBV,STHBV,XLIM,YLIM,
     3AMLIM,WLIM,PPLIM,THLIM,TLIM,PLIM,AMUL,SMLIM,CMLIM,TMLIM,THPM,
     4TANP,THMM,SINM,COSM,TANM,XATY,ACL,BCM,TEMP,WD,P,N,I,J,AREA,PRINT,
     5NAPRX,NN,ALNW,ALNP,STOR
     6,SINP,COSP
      THPX=THX+AMUX
      COSX=COSF(THPX)
      SINX=SINF(THPX)
      TANX=SINX/COSX
      RETURN
      END


      SUBROUTINE AMCMU(WX,SMUX,TMUX,AMUX,AMX,CMUX)
C     SUBROUTINE AMCMU COMPUTES MU AND M GIVEN W
      DIMENSION STOR(4000),TEMP(10),EMTAB(100),WTAB(100),WLOGT(100),
     1RHOLNT(100)
     2,TTAB(100),EMSQT(100)
      EQUIVALENCE (EMTAB,DUMMY1),(WTAB,DUMMY2),(WLOGT,DUMMY3),(RHOLNT,
     1DUMMY4),(TTAB,DUMMY5),(EMSQT,DUMMY6)
      COMMON EMTAB,WTAB,WLOGT,RHOLNT,TTAB,EMSQT
      COMMON XA,YA,THA,WA,FA,PSIA,XB,YB,THB,WB,XC,YC,THC,WC,FC,PSIC,AMC,
     1AMUC,SMUC,CMUC,TMUC,PPC,YAV,THAV,WAV,AMAV,AMUAV,SMUAV,CMUAV,TMUAV,
     2STHAV,YBV,THBV,WBV,AMBV,AMUBV,SMUBV,CMUBV,TMUBV,STHBV,XLIM,YLIM,
     3AMLIM,WLIM,PPLIM,THLIM,TLIM,PLIM,AMUL,SMLIM,CMLIM,TMLIM,THPM,
     4TANP,THMM,SINM,COSM,TANM,XATY,ACL,BCM,TEMP,WD,P,N,I,J,AREA,PRINT,
     5NAPRX,NN,ALNW,ALNP,STOR
     6,SINP,COSP
      OM=1./(WX*WX)
      CALL FTLUP(OM,OM,1,NN,WTAB(1),EMTAB(1))
      SMUX=SQRTF(OM)
      AMX=1./SMUX
      CMUX=SQRTF(1.-OM)
      TMUX=SMUX/CMUX
      AMUX=ATANF(TMUX)
      RETURN
      END


      SUBROUTINE GENPT
C     SUBROUTINE GENPT COMPUTES GENERAL POINT BY THREE DIMENSIONAL
C        IRROTATIONAL FLOW EQUATIONS MAKING AS MANY APPROXIMATIONS AS
C        DESIRED
      AVRGF(THA,THC)=.5*(THA+THC)
      DIMENSION STOR(4000),TEMP(10),EMTAB(100),WTAB(100),WLOGT(100),
     1RHOLNT(100)
     2,TTAB(100),EMSQT(100)
      EQUIVALENCE (EMTAB,DUMMY1),(WTAB,DUMMY2),(WLOGT,DUMMY3),(RHOLNT,
     1DUMMY4),(TTAB,DUMMY5),(EMSQT,DUMMY6)
      COMMON EMTAB,WTAB,WLOGT,RHOLNT,TTAB,EMSQT
      COMMON XA,YA,THA,WA,FA,PSIA,XB,YB,THB,WB,XC,YC,THC,WC,FC,PSIC,AMC,
     1AMUC,SMUC,CMUC,TMUC,PPC,YAV,THAV,WAV,AMAV,AMUAV,SMUAV,CMUAV,TMUAV,
     2STHAV,YBV,THBV,WBV,AMBV,AMUBV,SMUBV,CMUBV,TMUBV,STHBV,XLIM,YLIM,
     3AMLIM,WLIM,PPLIM,THLIM,TLIM,PLIM,AMUL,SMLIM,CMLIM,TMLIM,THPM,
     4TANP,THMM,SINM,COSM,TANM,XATY,ACL,BCM,TEMP,WD,P,N,I,J,AREA,PRINT,
     5NAPRX,NN,ALNW,ALNP,STOR
     6,SINP,COSP
      DO 51=1,NAPRX
      IF(I-1) 4,3,4
    3 THAV=THA
      THBV=THB
      WAV=WA
      WBV=WB
   30 CALL AMCMU(WAV,SMUAV,TMUAV,AMUAV,AMAV,CMUAV)
      CALL AMCMU(WBV,SMUBV,TMUBV,AMUBV,AMBV,CMUBV)
      CALL THP(THAV,TANP,COSP,AMUAV,THPM,SINP)
      CALL THM(THBV,TANM,COSM,AMUBV,THMM,SINM)
      STHAV=SINF(THAV)
      STHBV=SINF(THBV)
      XATY=XA*TANP-YA
      XC=(XATY+YB-XB*TANM)/(TANP-TANM)
      YC=XC*TANP-XATY
      ACL=SMUAV*TMUAV*STHAV/COSP
      BCM=SMUBV*TMUBV*STHBV/COSM
      YAV=AVRGF(YA,YC)
      YBV=AVRGF(YB,YC)
      IF(YAV+YBV) 1,2,1
    1 TEMP=-THA*TMUAV+(XC-XA)*ACL/YAV
      THC=(-WA-WAV*TEMP+WB+WBV*(THB*TMUBV+(XC-XB)*BCM/YBV))/
     1(WAV*TMUAV+WBV*TMUBV)
      WC=WA+WAV*(TMUAV*THC+TEMP)
      GO TO 5
```

```
    2 THC=(-WA+WB)/(2.*(WAV*TMUAV+WBV*TMUBV))
      WC=WA+WAV*2.*TMUAV*THC
      GO TO 5
    4 THAV=AVRGF(THA,THC)
      THBV=AVRGF(THB,THC)
      WAV=AVRGF(WA,WC)
      WBV=AVRGF(WB,WC)
      GO TO 30
    5 CONTINUE
      CALL AMCMU(WC,SMUC,TMUC,AMUC,AMC,CMUC)
      CALL PSI(WC,PPC)
      RETURN
      END



C     P-700.1
C     PART III COMPUTES BOUNDARY LAYER USING
C          WALL POINTS PUNCHED BY PART II
      DIMENSION FS(2),SUM(2),ANS(2),X(2000),Y(2000),W(2000),RRT(2000),
     1THF(2000),TI(2000),SVY(2000),SVDELT(2000),DELS(2000),YY(2000)
      COMMON OPT
      COMMON1,RRI,TO,THB,QSUM,QW,EN,ERR,UI,HW,R,HT,CON1,CON2,
     1CON,T,H,Q,FR,FPR,H3,HWS,K,RHOI,QI,X,Y,W,RRT,THF,SVY,SVDELT,DELS,YY
     2                    ,RHOT,VE,R1,C1,D1,E1,THI,GC,
     3    OMEGA,TW,     XM,TLTG,JLIM,DEBUG,N,L,ACASE,ALPHA,
     4BETA,GAM,TAU,PR,TTIG,X1,Y1,EM1,W1,RRT1,THF1,TI1,
     5                              TLTI,TT11,THETA,DXR,DU,
     6DR,DY,         PI,EMU,RETH,TEMP,FT,FTPR,H1,  DSDEL,
     7THDEL,TAW,ALP,CW,C2,C3,C4,FTT,FTTPR,H2,CF2,DSTH,
     8DTDX,YPD,DEL
     9         ,DP,CP,BP,AP,    HI
    1 WRITE OUTPUT TAPE 6,25
   25 FORMAT(1H 6X5HACASE13X4HRHOT14X2HVE15X2HR115X2HC115X2HD1
     115X2HE1/7X3HTHI15X2HGC15X1HR15X3HTHB
     213X5HOMEGA14X2HTW14X3HERR/8X2HXM14X4HTLTG
     312X5HALPHA13X4HBETA13X3HGAM14X3HTAU15X2HPR/
     47X4HTTIG14X2HTD15X2HAP15X2HBP15X2HCP15X2HDP15X2HHT)
  103 FORMAT(1H 7E17.8)
  100 FORMAT(1H06E17.8/6E17.8)
      CALL FINP(39,RHOT,VE,R1,C1,D1,E1,THI,GC,R,THB,OMEGA,
     1TW,ERR,XM,TLTG,JLIM,DEBUG,N,L,ACASE,ALPHA,BETA,GAM,
     2TAU,PR,TTIG,TO,AP,BP,CP,DP,HT,APP,BPP,CPP,YSTAR,
     3OPT,DIFN,DIFD)
      WRITEOUTPUTTAPE6,103,ACASE,RHOT,VE,R1,C1,D1,E1,THI,GC,R,THB,OMEGA,
     1TW,ERR,XM,TLTG,ALPHA,BETA,GAM,TAU,PR,TTIG
     2,TO,AP,BP,CP,DP,HT
   26 FORMAT(1H 8X1HX16X1HY14X5HTHETA13X4HCF/2
     114X1HN14X6HTH/DEL/5X7HY+DELST11X5HDELST13X3HDFL
     214X4HRETH13X4HTLTI10X9HDELST/DEL)
      J=JLIM
C     SUBROUTINE BIRD READS BINARY CARDS CONTAINING X,Y,M,W,RHO/RHOT,
C        THETA,T
C          LIMIT OF 2000 CARDS
C     READ IN WALL POINTS EXIT TO THROAT
C     MULTIPLY X AND Y BY XM AND STORE THROAT TOEXIT
 1000 CALL BIRD(X1,TI1)
      X(J)=X1*XM
      Y(J)=Y1*XM
      W(J)=W1
      RRT(J)=RRT1
      THF(J)=THF1
      TI(J)=TI1
      SVY(J)=Y(J)
   50 SVDELT(J)=0
      J=J-1
      IF(J)81,81,1000
   81 TLTI=TLTG
      TT11=TTIG
      THETA=THI
      WRITEOUTPUTTAPE6,26
      SENSE LIGHT 1
    2 DO80J=1,JLIM
      K=J
      RHOI=RRT(J)*RHOT
      UI=W(J)*VE
      PI=R1*TI(J)*RHOI
      EMU=(C1*(TI(J)**1.5))/((TI(J)**D1)+E1)
C     EQUATION B10
      IF(PI-20000.)203,203,204
  203 QI=1.
      GOTO4
  204 QI=PI*(PI*(PI*(TAU)+GAM)+BETA)+ALPHA
    4 IF(THB/TT11-24.)120,120,101
  101 FT=VE*VE-QI*(7.*TT11*R)
      FTPR=-QI*(7.*R)
      GOTO102
  120 TEMP=EXPF(THB/TT11)
      FT=VE*VE-QI*(7.*TT11*R+(2.*R*THB)/(TEMP-1.))
      FTPR=-QI*(7.*R+(((THB*THB*2.*R)/(TT11*TT11))*TEMP)
     1/((TEMP-1.)**2))
  102 H1=-FT/FTPR
      TT11=TT11+H1
      IF(ABSF(H1/TT11)-ERR)5,5,4
C     EQUATION B16
    5 IF(CPP)400,401,400
  401 TW=TT11
      GOTO402
  400 TW=(CPP-APP*(SVY(J)/YSTAR)**1.8)/(1.+BPP*(SVY(J)/YSTAR)**1.8)
```

```
C      EQUATION B11
  402 IF(PI-20000.)205,205,206
  205 QW=1.
      GOTO207
  206 QW=PI*(PI*(PI*(DP)+CP)+BP)+AP
  207 IF(THB/TW-24.)104,104,105
  105 HWS=(7.*TW)/(2.*T0)
      GOTO106
  104 HWS=(7.*TW)/(2.*T0)+THB/((EXPF(THB/TW)-1.)*T0)
  106 IF(THB/TI(J)-24.)107,107,108
  108 HI=(7.*TI(J))/(2.*T0)
      GOTO109
  107 HI=(7.*TI(J))/(2.*T0)+THB/((EXPF(THB/TI(J))-1.)*T0)
  109 QSUM=(QI-QW)/(HI-HWS)
      IF(THB/TW-24.)110,110,111
  111 HW=((7.*TW)/(2.*T0))*QW
      GOTO112
  110 HW=((7.*TW)/(2.*T0)+THB/((EXPF(THB/TW)-1.)*T0))*QW
  112 RET=(RHOI*UI)/(EMU*12.)
  503 RETH=RET*THETA
C      EQUATION B5
      EN=1.77*.43429448*LOGF(RETH)-.38-200./RETH
      IF(SENSELIGHT1)511,502
  502 IF(ABSF(EN-ENP)-DIFN)500,500,501
  511 SENSELIGHT1
  501 RRI=.125
C      SUBROUTINE GAUSS INTEGRATION 5 INTERVALS AND 32 POINTS PERINTERVAL
      CALL GAUSS(N,L,0.,1.,2,S,FS,SUM,ANS,3)
C      DELTA STAR/DELTA
      DSDEL=1.-ANS(1)
C      THETA/DELTA
      THDEL=1.-DSDEL-ANS(2)
      TAW=(PR**.33333333)*(TT1-TI(J))+TI(J)
      ALP=(1.+OMEGA)/(EN+1.)
      CW=TW/TI(J)
      C2=(TW-TAW)/TI(J)
      C3=(20.*EN*THDEL/RETH)**(1./(EN+1.))
      C4=(TAW-TI(J))/TI(J)
    7 FTT=CW-C2*C3*(TLTI**ALP)-C4*C3*C3*(TLTI**(2.*ALP))-TLTI
      FTTPR=-ALP*C2*C3*(TLTI**(ALP-1.))-2.*ALP*C4*C3*C3*
     1(TLTI**(2.*ALP-1.))-1.
      H2=-FTT/FTTPR
C      EQUATION B14
C      TL/TI
      TLTI=TLTI+H2
      IF(ABSF(H2/TLTI)-ERR)6,6,7
C      EQUATION B13
C      CF/2
    6 CF2=(1./(20.*EN))*C3*C3*((TLTI)**((1.+2.*OMEGA-EN)
     1/(EN+1.)))
C      DELTA STAR/THETA
      DSTH=DSDEL/THDEL
  500 DELS(J)=DSTH*THETA
      YPD=SVY(J)+DELS(J)
      DEL=DELS(J)/DSDEL
      WRITEOUTPUTTAPE6,100,X(J),Y(J),THETA,CF2,EN,THDEL,YPD,DELS(J),DEL,
     1RETH,TLTI,DSDEL
      YY(J)=Y(J)
      Y(J)=YPD
      IF(J-1)504,505,504
  505 DELSP=DELS(J)
      GOTO509
  504 DXB=(X(J)-X(J-1))/COSF(THE(J-1))
      DU=VE*(W(J)-W(J-1))
      DR=RHOI*(RRT(J)-RRT(J-1))
      DY=Y(J)-Y(J-1)
C      D THETA/D X
      DTDX=CF2P-THETAP*(((2.*DSTHP)*DU)/(UIP*DXB)+DR/(RHOIP*DXB)
     1+DY/(Y(J-1)*DXB))
      THETA=THETAP+(DTDX)*DXB
      IF(SENSELIGHT1)508,506
  506 IF(ABSF((DELS(J)-DELSP)/SVY(J))-DIFD)509,509,508
  508 DELSP=DELS(J)
      ENP=EN
      GOTO503
  509 Y(J+1)=Y(J+1)+DELS(J)
      CF2P=CF2
      THETAP=THETA
      DSTHP=DSTH
      UIP=UE
      RHOIP=RHOI
  510 SENSELIGHT1
   80 CONTINUE
 1001 XINT=0
      WRITE OUTPUT TAPE 6,514
C      USE SECOND ORDER INTERPOLATION TO FIND GIVEN POINTS
C      DX=.10 IF Y LESS THAN 1.
C      DX=.25 IF Y GREATER THAN 1. AND LESS THAN5.
C      DX=.50 IF Y GREATER THAN 5.
 1005 CALL FTLUP(XINT,YINT,2,JLIM,X,YY)
      WRITE OUTPUT TAPE 6,513,XINT,YINT
      IF(YINT-YY(JLIM))1006,1,1
 1006 IF(YINT-1.)1002,1009,1009
 1002 XINT=XINT+.1
      GO TO 1005
 1009 IF(YINT-5.)1003,1004,1004
 1003 XINT=XINT+.25
      GO TO 1005
 1004 XINT=XINT+.5
      GO TO 1005
  513 FORMAT(1H 2F12.4)
  514 FORMAT(1H 6X1HX11X1HY)
```

```
      END


      SUBROUTINEFOFX(S,FS)
      DIMENSION FS(2),SUM(2),ANS(2),X(2000),Y(2000),W(2000),RRT(2 0),
     1THF(2000),TI(2000),SVY(2000),SVDELT(2000),DELS(2000),YY(2000)
      COMMON OPT
      COMMONTI,RRI,T0,THB,QSUM,QW,EN,ERR,UI,HW,R,HT,CON1,CON2,
     1CON,T,H,Q,FR,FPR,H3,HWS,K,RHOI,CI,X,Y,W,RRT,THF,SVY,SVDELT,DELS,YY
      CON1=((UI*UI)/(R*T0))
      CON2=S**(1./EN)
      CON=CON1*(HW*(1.-CON2)/CON1+HT*CON2/CON1-.5*CON2*CON2)
C     ITERATE FOR RHO/RHOI
   11 T=TI(K)/RRI
C     IF EXPONENTIAL GREATER THAN 24. OMIT TERM
C     EQUATION B9
      IF(THB/T-24.)113,113,114
  114 H=(7.*T)/(2.*T0)
      GO TO 1152
  113 H=(7.*T)/(2.*T0)+THB/((EXPF(THB/T)-1.)*T0)
 1152 IF(OPT)115,1150,115
 1150 Q=QI
      GO TO 1151
  115 Q=(QSUM)*(H-HWS)+QW
C     IF EXPONENTIAL GREATER THAN 24. OMIT TERM
 1151 IF(THB*RRI/TI(K)-24.)116,116,117
  117 FR=Q*((7.*TI(K))/(2.*T0*RRI))-CON
      FPR=Q*((-7.*TI(K))/(2.*T0*RRI*RRI))
      GO TO 118
  116 FR=Q*((7.*TI(K))/(2.*T0*RRI)+THB/((EXPF(THB*RRI/TI(K))-1.)*T0))
     1-CON
      FPR=Q*((-7.*TI(K))/(2.*T0*RRI*RRI)-(THB*THB*EXPF(THB*RRI/
     1TI(K)))/(T0*TI(K)*(EXPF(THB*RRI/TI(K))-1.)**2))
  118 H3=-FR/FPR
C     EQUATION B12
      RRIN=RRI+H3
      IF(RRIN)125,125,126
  125 RRI=RRI*.5
      GO TO 11
  126 RRI=RRIN
      IF(ABSF(H3/RRI)-ERR)13,13,11
   13 FS(1)=RRI*(S**(1./EN))
   40 FS(2)=RRI*(S**(2./EN))
      HOLD=S
      HOLD2=FS(1)
   44 HOLD3=FS(2)
  100 FORMAT(1H 7E17.8)
      RETURN
      END
```

## REFERENCES


1. Guentert, Eleanor Costilow, and Neumann, Harvey E.: Design of Axisymmetric Exhaust Nozzles by Method of Characteristics Incorporating a Variable Isentropic Exponent. NASA TR R-33, 1959.

2. Enkenhus, K. R., and Maher, E. F.: The Aerodynamic Design of Axisymmetric Nozzles for High-Temperature Air. NAVWEPS Rep. 7395, U.S. Naval Ord. Lab. (White Oak, Md.), Feb. 5, 1962.

3. Erickson, Wayne D., and Creekmore, Helen S.: A Study of Equilibrium Real-Gas Effects in Hypersonic Air Nozzles, Including Charts of Thermodynamic Properties for Equilibrium Air. NASA TN D-231, 1960.

4. Young, A. D.: Boundary Layers. Vol. I of Modern Developments in Fluid Dynamics - High Speed Flow, L. Howarth, ed., The Clarendon Press (Oxford), 1953, pp. 375-475.

5. Persh, Jerome, and Lee, Roland: A Method for Calculating Turbulent Boundary Layer Development in Supersonic and Hypersonic Nozzles Including the Effects of Heat Transfer. NAVORD Rep. 4200 (Aeroballistic Res. Rep. 320), U.S. Naval Ord. Lab. (White Oak, Md.), June 7, 1956.

6. Ames Research Staff: Equations, Tables, and Charts for Compressible Flow. NACA Rep. 1135, 1953. (Supersedes NACA TN 1428.)

7. Hilsenrath, Joseph, Beckett, Charles W., et al.: Tables of Thermal Properties of Gases. NBS Cir. 564, U.S. Dept. Commerce, 1955, pp. 297-368.

8. Hall, N. A., and Ibele, W. E.: Thermodynamic Properties of Air, Nitrogen and Oxygen as Imperfect Gases. Tech. Paper No. 85, Eng. Exp. Station, Univ. of Minnesota, Dec. 1951.

9. Donaldson, Coleman duP.: Note on the Importance of Imperfect-Gas Effects and Variation of Heat Capacities on the Isentropic Flow of Gases. NACA RM L8J14, 1948.

10. Baradell, Donald L.: Experimental Verification of Boundary-Layer Corrections in Hypersonic Nozzles. Jour. Aero/Space Sci. (Readers' Forum), vol. 26, no. 7, July 1959, pp. 454-455.

11. McCracken, Daniel D.: A Guide to FORTRAN Programming. John Wiley & Sons, Inc., c.1961.

12. Ferri, Antonio: Elements of Aerodynamics of Supersonic Flows. The MacMillian Co., 1949.

13. Beckwith, Ivan E., Ridyard, Herbert W., and Cromer, Nancy: The Aerodynamic Design of High Mach Number Nozzles Utilizing Axisymmetric Flow With Application to a Nozzle of Square Test Section. NACA TN 2711, 1952.

14. Persh, Jerome: A Theoretical Investigation of Turbulent Boundary Layer Flow With Heat Transfer at Supersonic and Hypersonic Speeds. NAVORD Rep. 3854, U.S. Naval Ord. Lab. (White Oak, Md.), May 19, 1955.

15. Cohen, Nathaniel B.: A Method for Computing Turbulent Heat Transfer in the Presence of a Streamwise Pressure Gradient for Bodies in High-Speed Flow. NASA MEMO 1-2-59L, 1959.

16. Bartz, D. R.: A Simple Equation for Rapid Estimation of Rocket Nozzle Convective Heat Transfer Coefficients. Jet Propulsion (Tech. Notes), vol. 27, no. 1, Jan. 1957, pp. 49-51.



NASA-Langley, 1963 L-3180